10.2514/6.2024-0069

Investigation of Unconventional Coherent Structures in Implicit Large Eddy Simulations of Supersonic Turbulent Boundary Layers

Christian J. Lagares-Nieves[1,2*], Matthew Holland[2†] and Guillermo Araya[2‡]
[1]*Dept. of Mechanical Eng., University of Puerto Rico at Mayaguez, PR 00681, USA.*
[2]*Computational Turbulence and Visualization Lab., Dept. of Mechanical Eng., University of Texas at San Antonio, TX 78249, USA.*

We investigate the performance of numerically implicit subgrid-scale modeling provided by the well-known streamline upwind/Petrov-Galerkin (SUPG) stabilization for finite element discretization of advection-diffusion problems in a Large Eddy Simulation (iLES) approach. While its original purpose was to provide sufficient algorithmic dissipation for a stable and convergent numerical method, more recently it has been utilized as subgrid-scale (SGS) model to account for the effect of small scales, unresolvable by the discretization. These iLES modelling efforts are evaluated at very high Reynolds numbers ($Re_{\delta 2} \approx 10,800$) based on the freestream velocity, momentum thickness and wall viscosity or friction Reynolds number $\delta^+ \approx 2,500$. The freestream Mach number is 2.86. Direct comparison with a DNS database from our research group as well as with experiments and other DNS from the literature of adiabatic supersonic spatially-developing turbulent boundary layers (SDTBL) is performed. Focus is given to the assessment of the resolved Reynolds stresses, turbulent heat fluxes, and higher order statistics. The influence of coherent structures on the thermal transport phenomena is scrutinized via two-point cross-correlations of $u'v'$, $v'T'$ and $u'T'$. The employed numerical dissipation scheme, i.e. SUPG, as SGS model has demonstrated a good performance in the skin friction prediction as well as in high order statistics computation. Two-point cross-correlation of wall pressure fluctuations to domain pressure fluctuations reveals the presence of a "quadrupole" in the viscous sub-layer. In addition, two-point cross-correlation of velocity and thermal fluctuations has reported more noticeable volumes with high correlation values downstream of the reference point very close to the wall. On the other hand, those volumes with high velocity-thermal correlations displace upstream of the reference point (resembling very long and wall-attached tails) in the buffer and log regions. Furthermore, based on $R_{u'T'}$ structures, the high level of coherence observed between u' and T' implies that the Reynolds analogy still holds in supersonic turbulent boundary layers at $\delta^+ \approx$ 2,500.

I. Nomenclature

R_{δ_2}	=	Momentum thickness Reynolds number
M_∞	=	Freestream Mach number
U_∞	=	Freestream velocity
U^+_{VD}	=	Van Driest transform velocity in wall units
T_∞	=	Freestream temperature
T_r	=	Recovery temperature
T_w	=	Wall temperature
ν_w	=	Wall kinematic viscosity

*PhD Research Assistant & Doctoral Candidate, Department of Mechanical Engineering, 259 Alfonso Valdez Blvd., Mayaguez, PR, 00680, and Student Member, christian.lagares@upr.edu

†Graduate Research Assistant, Department of Mechanical Engineering, University of Texas at San Antonio, San Antonio, TX, 78249. AIAA Student Member, matthew.holland@my.utsa.edu

‡Associate Professor, Department of Mechanical Engineering, University of Texas at San Antonio, San Antonio, TX, 78249. AIAA Associate Fellow, araya@mailaps.org, https://ceid.utsa.edu/garaya/

u_τ	=	Friction velocity
P	=	Mean Pressure
T	=	Mean Temperature
k	=	Thermal conductivity
c_p	=	Specific heat at constant pressure
N_x	=	Number of Nodes Along the Streamwise Direction
N_y	=	Number of Nodes Along the Wall Normal Direction
N_z	=	Number of Nodes Along the Spanwise Direction
μ	=	Dynamic Molecular Viscosity
ρ	=	Fluid Density
δ	=	Boundary layer thickness
τ	=	Shear stress
Subscript	=	
inl	=	inlet
rec	=	recycle
$_{rms}$	=	Root-Mean Squared
$'$	=	Superscript denotes fluctuating components
∞	=	Subscript denotes freestream quantities

II. Introductory Remarks

The study of turbulent flows is of paramount importance as turbulence is prevalent in both scientific research and engineering applications. Among the various computational fluid dynamics (CFD) numerical techniques for addressing turbulence, Reynolds-Averaged Navier-Stokes (RANS), Large Eddy Simulation (LES), and Direct Numerical Simulation (DNS) are the most widely recognized approaches [1]. DNS directly solves the Navier-Stokes equations governing fluid flows without the need for any turbulence model. However, it requires substantial computational resources, often necessitating exceptional code scalability and efficiency [2]. Consequently, the execution of DNS, particularly when predicting spatially-developing turbulent boundary layers (SDTBL) requiring accurate time-dependent inflow conditions, demands expertise in high-performance computing (HPC) and parallel programming, including during the postprocessing stage [2].

Powerful supercomputers have facilitated the exploration of turbulent boundary layer simulations at higher Reynolds numbers via DNS [3–5]. In contrast, LES employs a spatial filter to model the effects of Kolmogorov scales [6], directly computing large-scale motions while only modeling small-scale motions. This results in reduced computational resources compared to DNS. However, the extent of this reduction is highly dependent on the analyzed geometry and flow complexity. In wall-bounded flows, even the inertial subrange scales situated in the near-wall region may be exceptionally small, and the computational effort reduction when employing LES relative to DNS may be limited to one order of magnitude in the spatial domain at most [7]. Nevertheless, LES allows for larger timesteps in unsteady simulations and CFL constraints, introducing an additional source of effort reduction.

Thus, LES can be defined as a **"DNS of large-scale motions"** by filtering out and modeling the turbulent scales below the inertial subrange. Although LES exhibits limitations in accurately reproducing peak values of flow fluctuations and Reynolds stresses in the buffer layer (i.e., for $y^+ \approx 15 - 20$, where turbulence production is at its maximum), it presents a promising alternative for computing the three-dimensional, time-dependent details of the largest turbulent structures, which govern most of the transport phenomena, by employing a simplistic model for the smaller turbulent scales. George and Tutkun [7] argue that the objectives of a closure solely dependent on grid-based filtering (or spectral truncation) are contingent upon the assumption of a spectral gap ensuring scale invariance. Additionally, they contend that attempting to utilize existing LES models at low Reynolds numbers or validating such models with current DNS data may be futile [7]. *Based on this argument, LES would only be meaningful at exceedingly high Reynolds numbers.* The landscape of LES modeling can be broadly categorized into two primary approaches [8, 9]:

- Explicit sub-grid scale (SGS) models: These models assume that the numerical method delivers an accurate solution for the resolved-scale equation, such as eddy-viscosity, scale-similarity, and mixed approaches. As they operate on the smallest represented scales, the models necessitate a minimal numerical truncation error, which can be reduced through spatial filtering.
- Implicit LES (iLES): This approach is characterized as an "implicit SGS" model, embedded within the numerical

discretization scheme. This integration is advantageous for addressing physically complex flows or intricate geometries, as it combines the numerical discretization with the SGS model. The primary distinction between iLES and traditional LES lies in the manner of SGS modeling [6]. Conventional LES incorporates a "physical" SGS model into the fluid dynamics calculation to account for unresolved turbulence scales, informed by the understanding of the structure and characteristics of turbulent flows. In contrast, iLES relies on the properties of a numerical method that adheres to a set of physical principles to achieve the same objective as explicit LES [6]. Empirical evidence has demonstrated the capacity of iLES to produce high-quality turbulence simulations [10–12].

Recently, the iLES approach has garnered considerable attention in the study of highly challenging high Reynolds number flows [6], where the employment of HPC tools is virtually obligatory. For example, the Monotone Integrated LES (MILES) approach, initially proposed by Boris [13], incorporates the effects of SGS physics on resolved scales via functional reconstruction of convective fluxes using locally monotonic finite volume schemes [14, 15]. The MILES method implicitly models the subgrid-scale stresses and turbulent heat fluxes through the numerical algorithm, integrating second-order or third-order accurate spatial schemes. Supersonic SDTBLs have been predicted through both explicit and implicit LES [16, 17], employing Lund et al.'s rescaling-recycling technique for turbulent inflow generation [18]. In [16], MILES and Smagorinsky models exhibited nearly identical results, suggesting that the Smagorinsky model was superfluous for supersonic turbulent boundary layers.

While the majority of the aforementioned studies utilized finite difference (FD) or finite volume (FV) numerical techniques, a growing body of research has explored turbulent boundary layers through continuous finite element methods [19–23]. Furthermore, Discontinuous Galerkin (DG) methods, first introduced by Reed and Hill [24] in 1973, have significantly advanced in recent decades, gaining prominence in computational fluid dynamics [25, 26]. Contrary to finite volume methods, DG methods enable higher-order accuracy on unstructured meshes [27, 28], facilitating efficient parallelization through hybridization [29, 30]. Additionally, DG methods demonstrate enhanced stability and robustness relative to continuous finite element methods [25, 26]. Moreover, the variational multiscale (VMS) method offers a finite element-specific, mathematically rigorous approach to LES [25, 31–33], with the availability of Sobolev subspaces enabling the spatial filtering operation in LES to be defined as a projection operation [25]. Recently, Stoter et al. [25] proposed a novel approach for incorporating discontinuous Galerkin methods into the variational multiscale paradigm for fluid dynamics problems.

In summary, this study aims to examine the numerical performance of implicit subgrid-scale modeling, utilizing the well-established streamline upwind/Petrov-Galerkin stabilization (SUPG) [19, 20] for finite element discretization of advection-diffusion problems in supersonic SDTBL at a freestream Mach number, M_∞, of 2.86. The investigation focuses on both traditional coherent structures and non-conventional coherent structures, such as those derived from two-point cross-correlations (TPCC) of $u'v'$, $v'T'$, and $u'T'$, as well as two-point correlation of wall-pressure fluctuation with v' and p' throughout a volume. The aim is to provide valuable insights into the efficacy of the iLES approach in the context of high Reynolds number flows and further inform the development of advanced computational fluid dynamics methodologies. To accomplish these objectives, we will leverage modern HPC resources, including large-scale parallelism and advanced numerical algorithms, to conduct simulations with an unprecedented level of detail. We will systematically compare the results of our iLES approach with those obtained from DNS (owned and external databases) and wind tunnel facilities, providing a comprehensive assessment of the relative merits and limitations of each method. This comparison will not only contribute to the validation of iLES as a practical tool for turbulent flow simulations but also shed light on the fundamental physical mechanisms governing turbulence generation, dissipation, and transport in supersonic SDTBL. By exploring the behavior of both traditional and non-conventional coherent structures in the context of iLES, our study will advance the understanding of the complex interplay between these structures and their role in the turbulence cascade. This knowledge will prove invaluable in the design of future turbulence models, as well as the development of flow control strategies for real-world engineering applications. Ultimately, this research will contribute to a broader scientific and engineering community's efforts to harness the full potential of iLES as a viable alternative to DNS and explicit LES for simulating turbulent flows in high Reynolds number regimes. By addressing the pressing need for more efficient and accurate computational methods in this challenging domain, our work will help pave the way for new discoveries and innovations in fluid dynamics, aerodynamics, and related fields.

III. Governing Equations and Inflow/Boundary Conditions

In this study, we investigate the behavior of compressible supersonic turbulent boundary layers (SDTBL) using the compressible Navier-Stokes equations, assuming low Knudsen numbers and neglecting non-equilibrium effects [34]. The

conservation of mass becomes non-trivial in compressible flows, especially when strong pressure gradients, compression, and expansion waves are present, causing abrupt variations in density. We describe, for reader's convenience, the classical conservation equations for mass, momentum, and energy in Equations 1, 2, and 3, respectively.

$$\frac{\partial \rho}{\partial t} + \frac{\partial}{\partial x_j}\left(\rho u_j\right) = 0 \tag{1}$$

$$\frac{\partial \rho u_i}{\partial t} + \frac{\partial}{\partial x_j}\left(\rho u_i u_j + p\delta_{ij} - \sigma_{ij}\right) = 0 \tag{2}$$

$$\frac{\partial \rho e}{\partial t} + \frac{\partial}{\partial x_j}\left((\rho e)u_j - u_i\sigma_{ij} + q_j\right) = 0 \tag{3}$$

where ρ is the density; u_i is the velocity in the i direction; p is the pressure; σ_{ij} is the stress tensor which we model as a linear stress-strain relationship,

$$\sigma_{ij} = 2\mu S_{ij} - \frac{2}{3}\mu\delta_{ij}S_k k \tag{4}$$

where $S_{ij} = \frac{1}{2}\left(\frac{\partial u_i}{\partial x_j} + \frac{\partial u_j}{\partial x_i}\right)$ is the strain rate tensor, μ is the kinematic viscosity; and q_i is the hear flux due to thermal gradients in the i direction and is modelled in the present work by Fourier's law, $q_i = \kappa\frac{\partial T}{\partial x_i}$ where κ is the thermal conductivity; e is total energy per unit mass which we assume to follow:

$$e = c_v T + \frac{1}{2}u_i u_j \tag{5}$$

where c_v is the specific heat at constant volume. Finally, we also assume the fluid viscosity to vary following a Power Law (see Equation 6).

$$\mu = \mu_\infty \left(\frac{T}{T_\infty}\right)^{0.76} \tag{6}$$

The 0.76-power law variation of the dynamic fluid viscosity has shown an excellent performance in our iLES predictions, with similar outcomes as for the well known Sutherland's viscosity law (which, in fact, also contains a 3/2 power law of the static temperature). However, equation 6 is more appropriate in the solution of the non-dimensional governing equations of the flow.

The strong form of the equations is presented, while the weak form is employed in the finite element solver. This study utilizes the PHASTA flow solver [35]. The finite element scheme is constructed on the basis of the streamline upwind Petrov-Galerkin (SUPG) finite element discretization in space, offering second-order accuracy [19, 20]. This numerical dissipation functions as an implicit subgrid scale (SGS) model. The non-linear system of equations is solved using an iterative Krylov solver in space, while maintaining full implicitness in time (2^{nd} order accurate). For further information on the finite element method used, readers are referred to [36, 37].

To effectively model the physics of SDTBL via iLES, several critical aspects must be considered: (i) the computational domain should be sufficiently large to accommodate the largest scale motions (LSM) or "superstructures" [38, 39]; (ii) accurate unsteady inflow turbulent fluctuations must be introduced [40, 41]; and (iii) the turbulent inflow fluctuations should exhibit the appropriate power spectrum to minimize the "inlet developing section" (ideally, this section should span 2-3 δ_{inl}'s). Proper turbulent inlet conditions enable the simulation of even larger Reynolds numbers (i.e., large scale systems), as resolving the laminar-transition stage is no longer necessary, thus optimizing the streamwise domain length by reducing the "non-physical" developing section. In this article, the Dynamic Multiscale Approach (DMA) for inlet generation, proposed by Araya *et al.* [40], is employed. This method has been extended to compressible SDTBL in [41–43], and is a modified version of the rescaling-recycling technique by Lund *et al.* [18]. Moreover, the proposed inflow condition generation method for compressible turbulent boundary layers has been recently demonstrated to be highly robust, with a minimal development region [44] (at most $2.5\delta_{inlet}$) and an energy spectrum resembling that of fully developed flow. Notably, the selection of outflow conditions was found to have a more significant impact on the quality of the energy spectrum. Compressible boundary layer extensions have also been proposed by Urbin & Knight [16], Stolz & Adams [17], and Xu & Martin [45]. The current inflow generation technique circumvents

the use of empirical correlations linking the inlet friction velocity to the recycle friction velocity, which will be further discussed in the manuscript. Figure 1 depicts an infographic representation of the DMA method, illustrating iso-contours of instantaneous static temperature normalized by the freestream temperature. The fundamental concept of the rescaling-recycling method involves extracting the flow solution (mean and fluctuating components of velocity, thermal, and eventually, pressure fields for compressible flows) from a downstream plane (termed "recycle") and, after applying scaling functions, reintroducing the transformed profiles at the inlet plane, as depicted in Figure 1. *Indeed, it has been reported that merely fixing the mean pressure at the inlet plane yielded more stable and accurate numerical cases than incorporating pressure fluctuations*. Our findings align with this conclusion. As stated in [46] and [16], "the static pressure can be assumed constant at the inlet plane since the pressure fluctuations are small compared to the static temperature fluctuations." Instantaneous density profiles (mean plus fluctuations) are indirectly imposed due to the equation of state for a perfect gas, which can be visually verified from Figure 1. The primary objective of implementing scaling laws to the flow solution is to transform the streamwise in-homogeneity of the flow into quasi-homogeneous conditions. This study focuses on employing the PHASTA flow solver and the SUPG finite element discretization for the numerical simulation of compressible SDTBL. The iLES approach, combined with the DMA method for inlet generation, ensures accurate representation of the turbulent flow properties. By considering the critical aspects of computational domain size, unsteady inflow turbulent fluctuations, and proper power spectrum of the fluctuations, a robust and reliable simulation of high Reynolds number flows can be achieved. The DMA method avoids using empirical correlations and is capable of providing accurate and stable numerical results, even for compressible flows. Future work may explore the impact of various outflow conditions on the quality of the energy spectra, as well as further extensions and improvements to the compressible boundary layer modeling approaches. The Reynolds decomposition is implemented for instantaneous parameters, i.e. a time-averaged plus a fluctuating component:

$$u_i(\mathbf{x}, t) = U_i(x, y) + u_i'(\mathbf{x}, t) \tag{7}$$

$$t(\mathbf{x}, t) = T(x, y) + t'(\mathbf{x}, t) \tag{8}$$

The SDTBL can be split into inner and outer zones, with distinct scaling laws applied in a multiscale manner [40]. A blending or weight function is utilized to generate composite instantaneous flow profiles, smoothly merging the contributions from the inner and outer zones. The projection of flow parameters from the recycle plane to the inlet is conducted along constant values of y^+ (inner region) and y/δ (outer region). Figure 1 additionally illustrates the schematic of the computational domain in the supersonic regime at very high Reynolds numbers. During the re-scaling process of the flow parameters [40], the ratio of the inlet friction velocity to the recycle friction velocity (i.e., $\lambda = u_{\tau,inl}/u_{\tau,rec}$) is required. The friction velocity is defined as $u_\tau = \sqrt{\tau_w/\rho}$, where τ_w represents the wall shear stress and ρ denotes the fluid density.

Since the inlet boundary layer thickness must be prescribed according to the predicted inlet Reynolds number, prescribing the inlet friction velocity becomes redundant. To address this issue, Lund *et al.* [18], Urbin & Knight [16], and Stolz & Adams [17] utilized the well-established one-eighth power law connecting the friction velocity to the momentum thickness in zero-pressure gradient flows, resulting in $u_{\tau,inl}/u_{\tau,rec} = (\delta_{2,inl}/\delta_{2,rec})^{-1/8}$. The empirical power (-1/8) may be significantly influenced by the Reynolds number dependency and compressibility effects. Consequently, we dynamically computed this power exponent, denoted as $\gamma_{\delta 2}$, "on the fly" by relating the mean flow solution from a new plane (referred to as the "Test" plane, as depicted in Figure 1) to the solution from the recycle plane as follows:

$$\gamma_{\delta 2} = \frac{ln(u_{\tau,test}/u_{\tau,rec})}{ln(\delta_{2,test}/\delta_{2,rec})}. \tag{9}$$

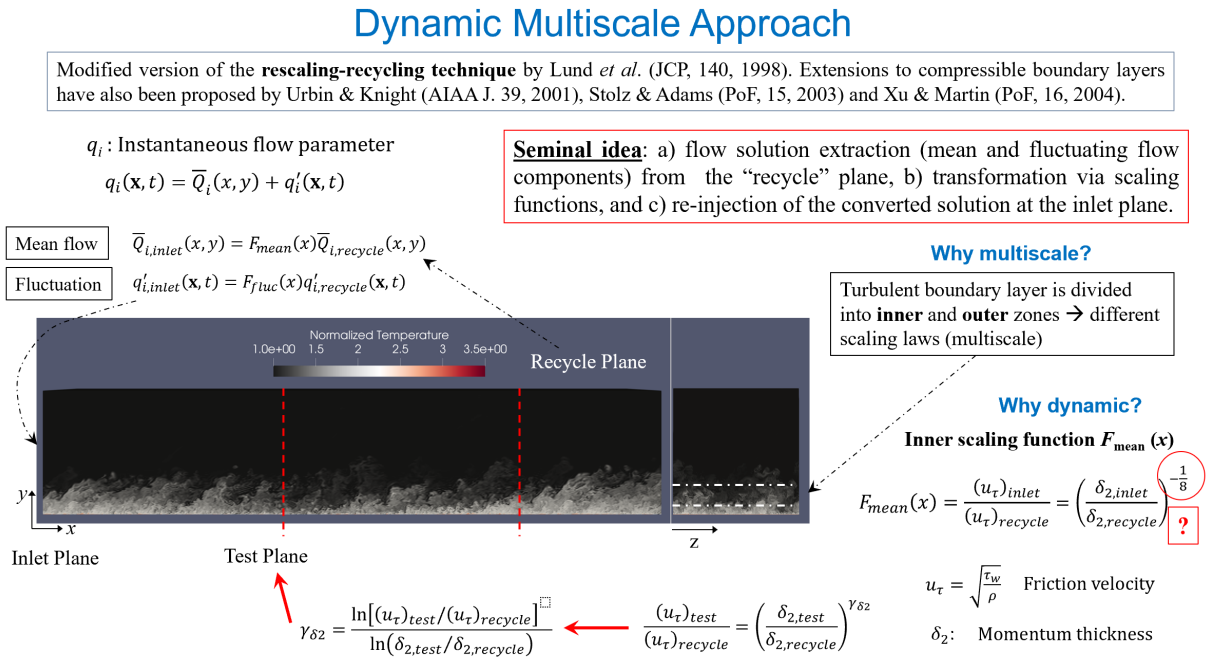

Fig. 1 Boundary layer schematic for the supersonic turbulent boundary layer at high Reynolds numbers. Contours of instantaneous static temperature.

Finally, in figure 1 it can be observed typical "bulges" and "valleys" as in incompressible turbulent boundary layers, with outer irrotational flow penetrating further into the near wall region. It is worth highlighting the very "fine" structure of turbulence at this high Reynolds number, where the flow becomes highly isotropic. This is consistent with findings by [5] via DNS of supersonic SDTBL at a Mach number of 2.

A. The Flow Solver for HPC

To effectively conduct the proposed DNS at high Reynolds numbers, a CFD solver with exceptional accuracy, efficiency, and scalability is necessary. PHASTA, an open-source, parallel, hierarchic (2^{nd} to 5^{th} order accurate), adaptive, and stabilized (finite-element) transient analysis tool, has been developed for solving compressible [36] and incompressible flows [19, 20]. By combining minimal dissipation numerics with adaptive [47–49] unstructured meshes, PHASTA has been successfully applied to a wide range of flows, from DNS and LES benchmarks such as channel flow and decay of isotropic turbulence [19, 22, 23, 50], to cases of practical interest encompassing incompressible [21, 51] and compressible [41, 49, 52–54] boundary layer flow control, as well as hypersonic flows [42, 43]. Consequently, PHASTA has established a robust record of supporting closely coordinated experimental-computational studies [49, 51–54]. PHASTA has been demonstrated [20] to be an effective tool for bridging a wide range of time and length scales in various flows, including turbulent ones, using implicit techniques (based on URANS, DDES, LES, DNS). Moreover, PHASTA has been meticulously designed for parallel performance [21, 55]. Figure 2 (a) presents isosurfaces of the Q criterion for vortex core identification over a vertical airplane tail with active flow control. Figure 2 (b) illustrates the scaling of PHASTA up to 786,432 cores (employing 1, 2, and 4 processes per core to leverage 4-way SMP, exceeding 3 million processes) in a 92 billion finite-element mesh. PHASTA has also been successfully ported and scaled on GPU-based and XEON-phi based machines. This unprecedented portable scaling within the CFD community is crucial for extending the proposed simulations to relevant Reynolds numbers.

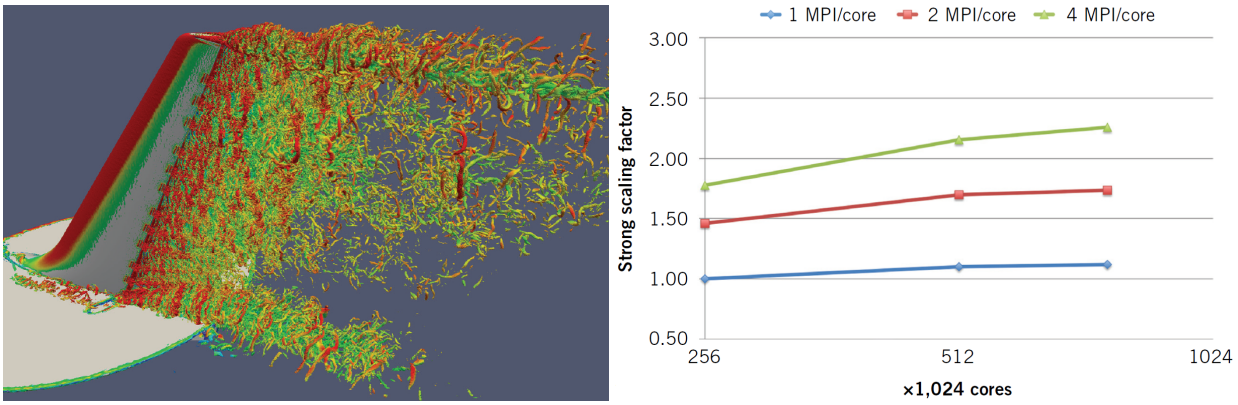

(a) (b)

Fig. 2 (a) Flow visualization in the wake of a deflected flap of a realistic two component wing assembly with active flow control (isosurfaces of instantaneous Q criterion colored by speed) and (b) scaling of PHASTA with 1, 2 and 4 MPI processes per core on the 92-billion element mesh. Adapted from Rasquin *et al.* [56].

IV. Postprocessing of Big Data

To cope with the growing demands of processing larger computational domains and gather valuable insight from large scale simulations, we have developed a scalable, out-of-core post-processing library capable of scaling from laptops to workstations to small clusters to large scale facilities equipped with both CPUs and GPUs. Aquila [57] is currently in its second iteration with a third major revision currently being developed. Figure 3 highlights the software structure for our post-processing solution which we call Aquila. The name comes from the latin for eagle and serves as a constant reminder that domain experts should not be required to dabble with low level computational nuances to gather scientific insight and should "fly" over these as high as possible while retaining excellent performance and scalability in the same way that eagles avoid storms by flying over them.

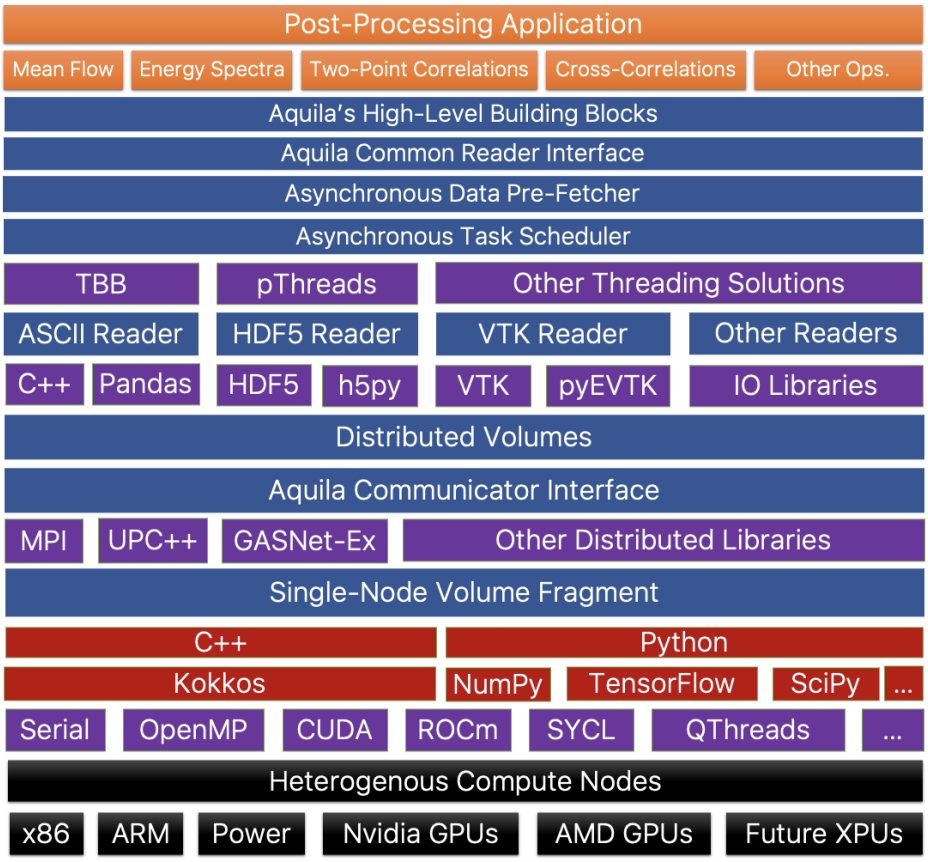

Fig. 3 High level schematic of the software components for Aquila.

In its current state, Aquila targets TensorFlow [58], the popular machine learning (ML), as its compute backend from Python. This enables transparent targeting of CPUs and GPUs from multiple vendors with excellent performance. Domain decomposition is done via MPI [59] as these implementations are often highly tuned in large scale computing facilities. Figure 4 depicts Aquila's strong scaling across both CPUs and GPUs. The user does not need to change anything in its scripts to target either GPUs or CPUs as this is all handled by TensorFlow. Aquila's scaling is assessed by computing the meanflow and a collection of "Quantities of Interest" (QoI) that include: fluid velocity, pressure and thermal fluctuations, boundary layer parameters (such as boundary layer thickness and its integral moments, friction velocity, skin friction coefficient, turbulent kinetic energy, 30 cross-correlations, third & fourth order moments, 20 full 3D two-point correlations and 1,237,500 spanwise energy spectra. The input dataset consisted of $\tilde{4}000$ flow fields which totaled approximately 8.3 TBs of database. Thus, operating with this data in-memory is impractical at low node counts or with typical node configurations. Aquila operates on this data on "cold" storage media and provides an illusion of an in-memory implementation by pre-fetching data asynchronously. In summary, Aquila achieves an excellent strong scaling performance with a parallel scaling efficiency above 80% and with the GPU runtime being 2 times faster. GPUs tend to shine on throughput oriented tasks as clearly seen in fig. 4 where the meanflow performance is entirely IO bound and the performance difference between the CPU and GPU is negligible whereas a significant difference is seen for the core portion of the benchmark. The asynchronous prefetcher yields a 23-24% improvement in total runtime. The combined speedup of using a pre-fetcher and an optimized GPU backend is approximately 2.48 times (considering a CPU-only backend without prefetching).

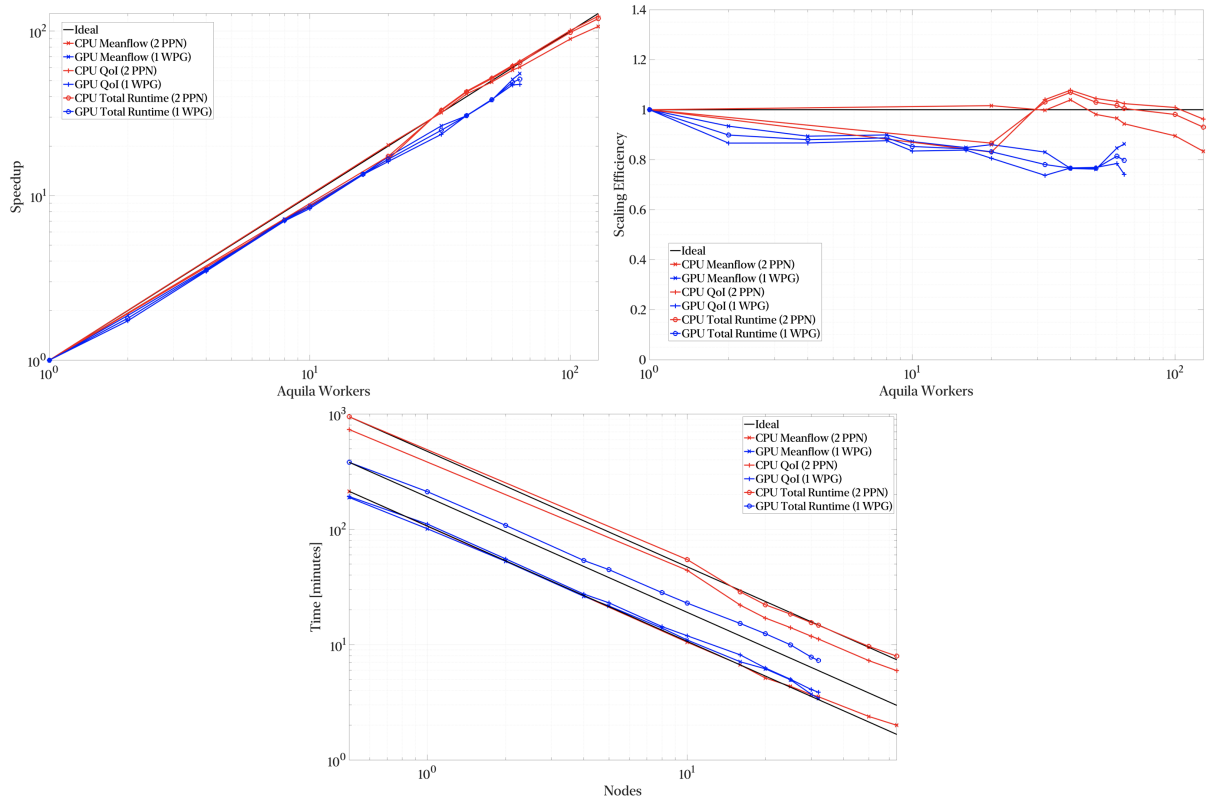

Fig. 4 Strong scaling behavior for Aquila (top-left); in CPU-only nodes, we fixed 2 processes per node and threaded across the remaining CPU cores (top-right); GPU nodes had 2 GPUs, and we allocated one rank per GPU ensuring a total of 2 MPI ranks (Workers) per node (bottom).

V. Mean flow and higher order statistics

Table 1 summarizes the characteristics of the analyzed iLES supersonic case. The number of flow fields employed in statistics computation, freestream Mach number, wall thermal condition (adiabatic), Reynolds number range (momentum and friction Reynolds numbers), computational domain dimensions in terms of the inlet boundary layer thickness δ_{inl} (where L_x, L_y and L_z represent the streamwise, wall-normal and spanwise domain length, respectively) and mesh resolution in wall units (Δx^+, $\Delta y^+_{min}/\Delta y^+_{max}$, Δz^+) are depicted by Table 1 The iLES case contains the following grid point numbers: $990 \times 250 \times 210$ (roughly a 52-million point mesh) along the streamwise, wall-normal and spanwise direction, respectively. This cases were run in 1200 processors at the Onyx supercomputer (ERDC, DoD).

Table 1 Numerical details of iLES case.

Regime	**Flow fields**	M_∞	T_w/T_∞	$Re_{\delta 2}$	δ^+	$L_x \times L_y \times L_z$	Δx^+,$\Delta y^+_{min}/\Delta y^+_{max}$, Δz^+
Supersonic	4001	2.86	2.74	9505-10835	2159-2510	$15\delta_{inl} \times 3\delta_{inl} \times 3\delta_{inl}$	32.8, 1.25/56, 31

A. Mean Flow

Figure 5 exhibits the streamwise development of the skin friction coefficient of present iLES supersonic data at a freestream Mach number of 2.86. It is worth noting the excellent agreement of present C_f results of iLES with a power-law curve fitting (i.e., $C_f = 0.0185 Re_{\delta 2}^{-0.29}$) based on experiments at similar Mach numbers from Stalmach [60]. In addition, C_f values at Mach 2.86 are included from DNS of Lagares & Araya (2022) [44] at much lower Reynolds

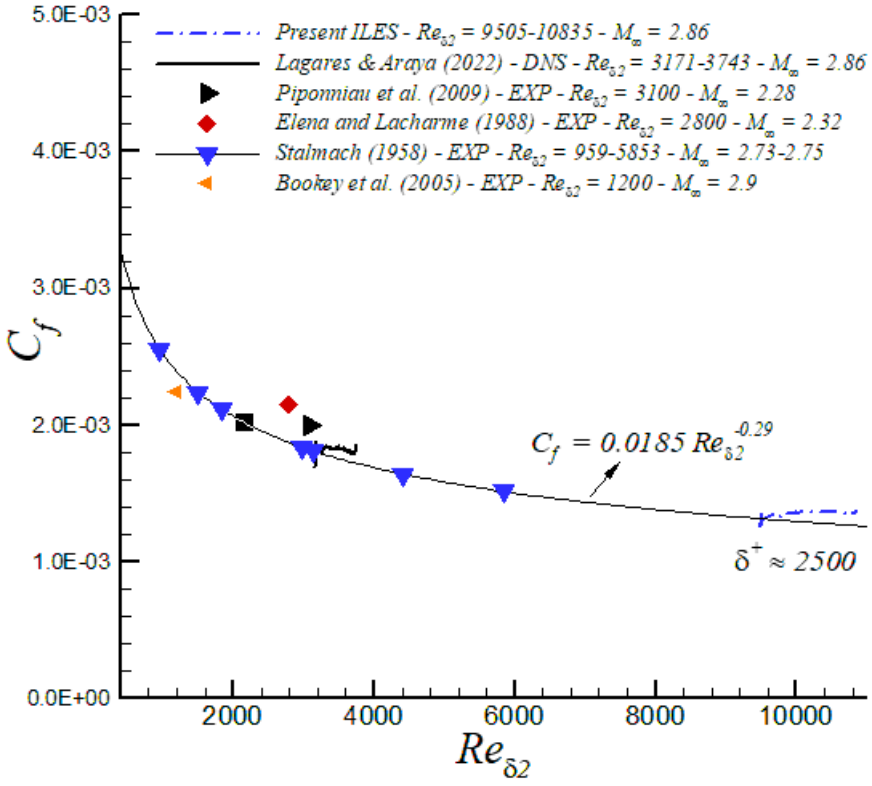

Fig. 5 Skin friction coefficient, C_f, in the supersonic flow regime.

numbers (about 3X lower). Furthermore, experimental data from [61], [62], [63] are also included at supersonic Mach numbers between 2 to 3, and at lower Reynolds numbers. For those low Reynolds number cases, the power-law curve fitting displays a very good performance, with the exception of experimental data by [62] with an almost 10% discrepancy. In fig. 6, the time-averaged streamwise velocity is plotted at a streamwise location where the local friction Reynolds number, δ^+, is 2430. The agreement with hot-wire anemometry data at a supersonic blowdown wind tunnel by Donovan et al. [64] is excellent, particularly in the outer region for $y/\delta > 0.03$ (or $y^+ > 250$). In fig. 7, both log and power laws have been evaluated via diagnostic functions, i.e. DF_{log} and DF_{power}. It is important to highlight that constant values of those diagnostic functions inside the boundary layer indicate the local presence of either log or power law behavior. Interestingly, a power law of U^+_{VD} occupies a slightly larger portion in the supersonic boundary layer, approximately extending between $115 < y^+ < 833$ or about 717 wall units. A 0.2% deviation of the normalized wall normal gradient of the diagnostic functions were considered in the log/power law assessment. Figure 8 shows second order statistics. In fig. 8 (a) the streamwise component of the resolved Reynolds normal stresses as well as the resolved Reynolds shear stresses are depicted at the middle of the computational domain. There is a clear over-prediction of $u'u'$ peaks by iLES, and ongoing investigation is being carried out to implement a more efficient numerical dissipation approach in the near wall region of the turbulent boundary layer. At such high Reynolds numbers, the constant shear layer or "plateau" is quite evident and large on the $u'v'$ profile. Interestingly, by looking at the turbulent heat fluxes from fig. 8 (b) one can infer a high level of similarity between $u'u'$ and $u'T'$ profiles, meaning that the Reynolds analogy still holds for those two correlations in supersonic turbulent boundary layers over adiabatic flat plates.

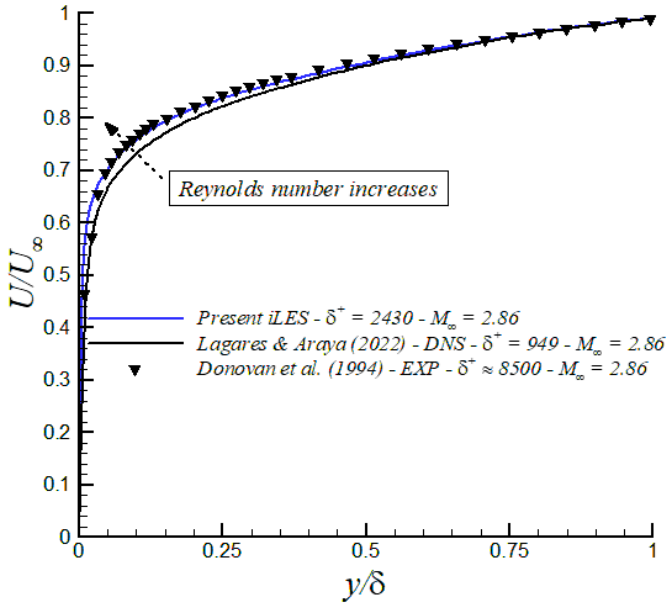

Fig. 6 Time-averaged streamwise velocity in outer units.

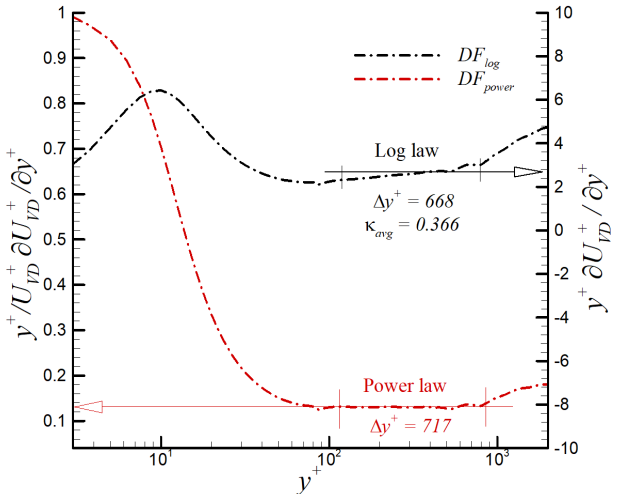

Log law

$$U_{VD}^{+} = \frac{1}{\kappa}\ln y^{+} + B \longrightarrow DF_{log} = y^{+}\frac{\partial U_{VD}^{+}}{\partial y^{+}}$$

Power law

$$U_{VD}^{+} = C(y^{+})^{\gamma} \longrightarrow DF_{power} = \frac{y^{+}}{U_{VD}^{+}}\frac{\partial U_{VD}^{+}}{\partial y^{+}}$$

Criterium to determine extension of Log/Power law in U^{+}_{VD}: 0.2% deviation of normalized $\partial DF/\partial y^{+}$

Fig. 7 Diagnostic functions for Log and Power law in supersonic regime at very high Reynolds numbers in iLES and M_∞ = 2.86.

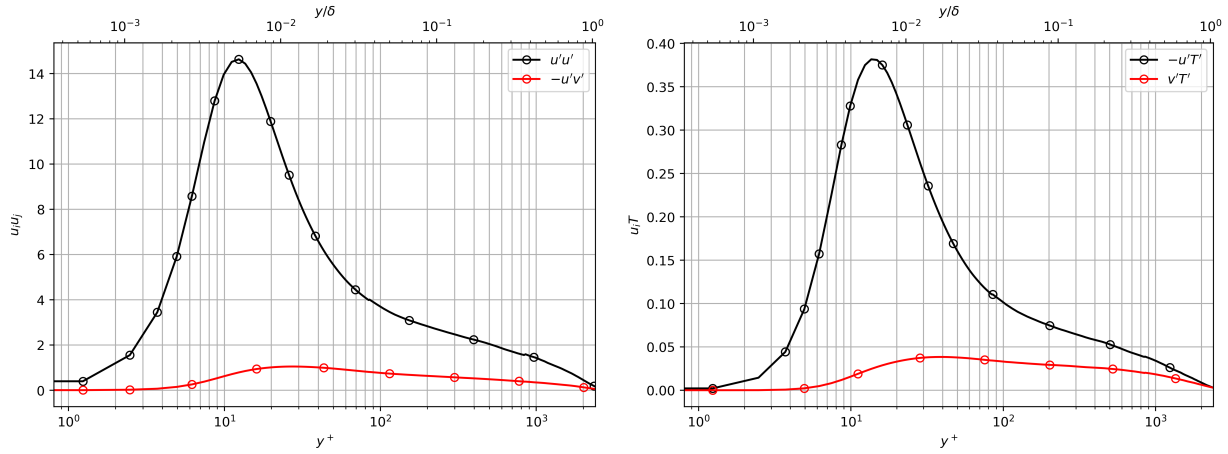

(a) (b)

Fig. 8 (a) Streamwise component of the Reynolds normal stresses and Reynolds shear stresses, (b) streamwise and wall-normal turbulent heat fluxes.

B. Higher-Order Statistics

Turbulence, a ubiquitous phenomenon characterized by its chaotic, random, and multi-scale nature, manifests several intriguing statistical properties. Among these properties, skewness, flatness, and intermittency stand out as particularly important for understanding the complexity and rich dynamics of turbulent flows [65]. Skewness and flatness, the third and fourth statistical moments respectively, serve as measures of the asymmetry and peakedness of a distribution. In the context of turbulence, a skewness value of zero would indicate a symmetric, likely Gaussian distribution of the turbulent fluctuations. Non-zero skewness, on the other hand, highlights the asymmetry of the distribution, potentially indicating the existence of dominant, one-sided fluctuations in the flow field [66]. Flatness, on the other hand, serves as an indicator of the presence of extreme, high-amplitude events. In a Gaussian distribution, the flatness equals 3. Higher flatness values in turbulence thus signify the occurrence of intense, sporadic events, leading to a distribution with heavier tails compared to the Gaussian [66]. These sporadic, intense events in turbulent flows are a manifestation of intermittency, an inherent property of turbulence. Intermittency refers to the localized, sporadic occurrence of intense, high-amplitude events in turbulent flows, leading to deviations from the classical Kolmogorov 1941 self-similar, scale-invariant energy distribution in the inertial subrange [65, 67]. Intermittency significantly influences the statistical properties of turbulence, leading to non-Gaussian behavior of turbulent fluctuations. This is often captured through the aforementioned higher order statistical moments. Furthermore, intermittency plays a crucial role in the energy cascade process in turbulence, leading to a modification of the energy spectrum, particularly in the high wave number or small scale regime. This phenomenon is often described by the concept of multifractality [65, 68]. Multifractality is a concept that originates from the field of fractal mathematics and has found significant application in the study of turbulence, including turbulent boundary layers. In general, a fractal is a geometric shape that is self-similar, meaning it appears the same at any scale. If you zoom in or out on a fractal, you will see the same pattern repeating over and over again. However, in many real-world systems, including turbulence, this self-similarity is not perfect. Instead, different parts of the system exhibit self-similarity with different scaling laws. This is where the concept of multifractality comes in. In the context of turbulence, multifractality refers to the idea that the statistical properties of turbulence (such as the distribution of energy among different scales of motion) are not uniform across all scales, but instead vary in a way that itself exhibits fractal behavior. This is particularly relevant in the study of turbulent boundary layers, where a wide range of scales of motion are present, from the large-scale motions influenced by the overall flow down to the small-scale motions near the wall where viscous effects become important. The concept of multifractality provides a framework for understanding and quantifying this scale-dependent behavior. It suggests that the turbulence is composed of a multitude of different "fractal dimensions", each associated with a different scale of motion. This multifractal nature of turbulence has significant implications for the energy cascade process, the mechanism by which energy is transferred from large scales of motion to smaller scales in a turbulent flow. It suggests that this process is not uniform, but instead varies across different scales in a way that reflects the multifractal structure of the turbulence.

Figure 9 showcases the intermittency throughout the boundary layer in outer units, i.e. as a function of y/δ. According to [69], the intermittency factor γ is defined as 3/F(u), where F(u) is the flatness of the streamwise velocity fluctuations. We have also included DNS data by Bernardini & Pirozzoli [5] at a freestream Mach number of 3 and $\delta^+ = 502$, thus, at a much lower Reynolds number than present iLES. The Reynolds number dependency is pretty evident in the very near wall region, with a γ-peak value much closer to the wall for present iLES at larger Reynolds numbers (our δ^+ is approximately four timer larger than that of [5]). In the outer region for $y/\delta > 0.1$, there is a very good agreement between our iLES results and DNS from [5]. The empirical curve fitting (power law) based on experimental data by [69] at significantly high Reynolds number is also included. We assess that the discrepancy in the outer region of the boundary layer is likely attributable to the Reynolds number difference since a clear trend towards the empirical correlation is seen as Re grows from the data reproduced from [5] to the present iLES data. Nonetheless, the general trends are consistent across all three curves where a mostly Gaussian behavior can be seen (note almost unitary values for γ in the region $0.1 < y/\delta < 0.6$). This breaks down as the fluid approaches the edge of the boundary layer. To further dissect the statistical nature of the boundary layer, the skewness and flatness are shown for pressure (fig. 10), streamwise velocity (fig. 11), wall-normal velocity (fig. 12) and temperature (fig. 13) fluctuations. Looking into figure 11, we note that although the flatness (inversely proportional but directly related to the intermittency) suggests a Gaussian trend, the distribution is negatively skewed hence pointing to low speed streaks being common throughout the boundary layer but especially so in the outer region. Now, accounting for the positive skewness of the wall-normal velocity in fig. 12 suggests that the flow has a high number of ejection events in the outer layer of the boundary layer. Although some ejections might originate in the inner layer, they appear to be far less common that in the outer portion. The inner layer of the boundary layer also resembles much more closely a Gaussian distribution which breaks down as the edge of the boundary layer is reached. Furthermore, pressure fluctuations appear to be much more violent with its values spread over a wider range as can be seen from figure 10b. On the other hand, the skewness suggests extreme low-pressure events are common throughout the boundary layer but especially so in the outer region. This is consistent with the prevalence of ejections since ejection events create a "void" to be filled by other fluid parcels (sweeps). The thermal fluctuations tend to show a similar behavior in terms of the flatness of the distribution (fig. 13b). The thermal boundary layer does exhibit strong "cooling" events near the vicinity of the wall and "heating" events as the flow approaches the edge of the boundary layer. The notable similarity between F(u) and F(T) suggests a kind of Reynolds analogy for those variables in supersonic turbulent boundary layers. On the other hand, there is a perfect asymmetry between S(u) and S(T).

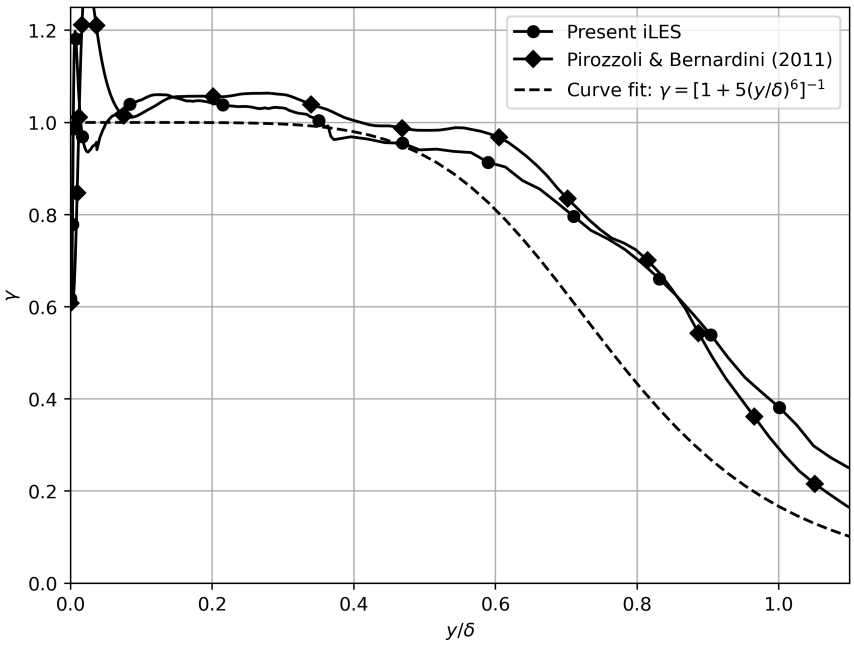

Fig. 9 Streamwise velocity fluctuations intermittency factor γ. Curve-fitting is based on experimental data by [69] as reproduced by [70].

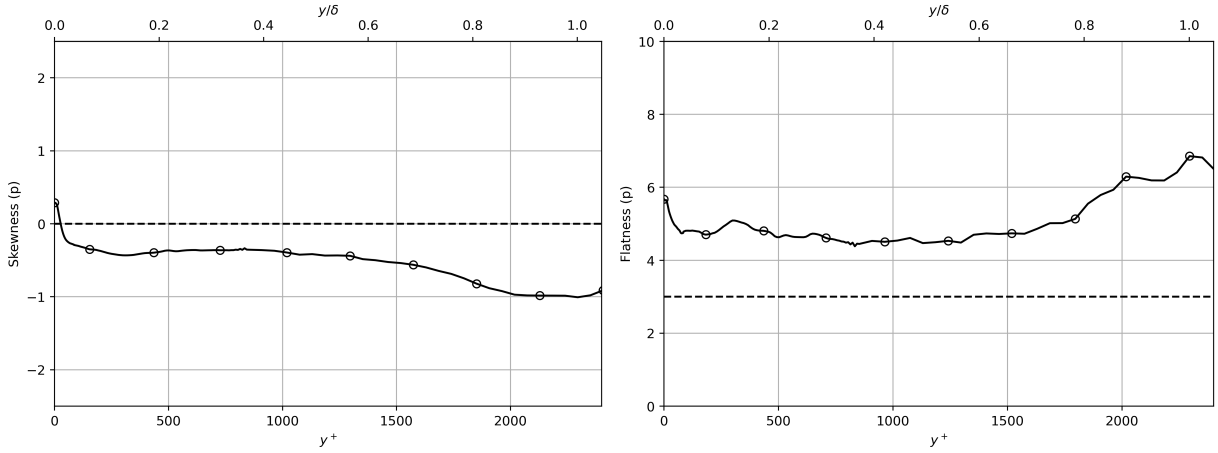

Fig. 10 Skewness and Flatness for the pressure fluctuations.

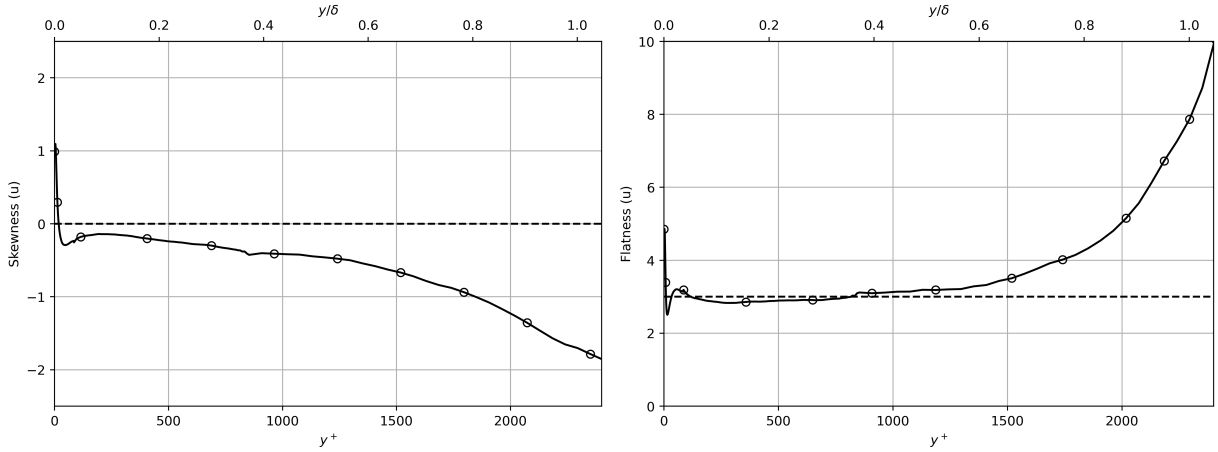

Fig. 11 Skewness and Flatness for the streamwise velocity fluctuations.

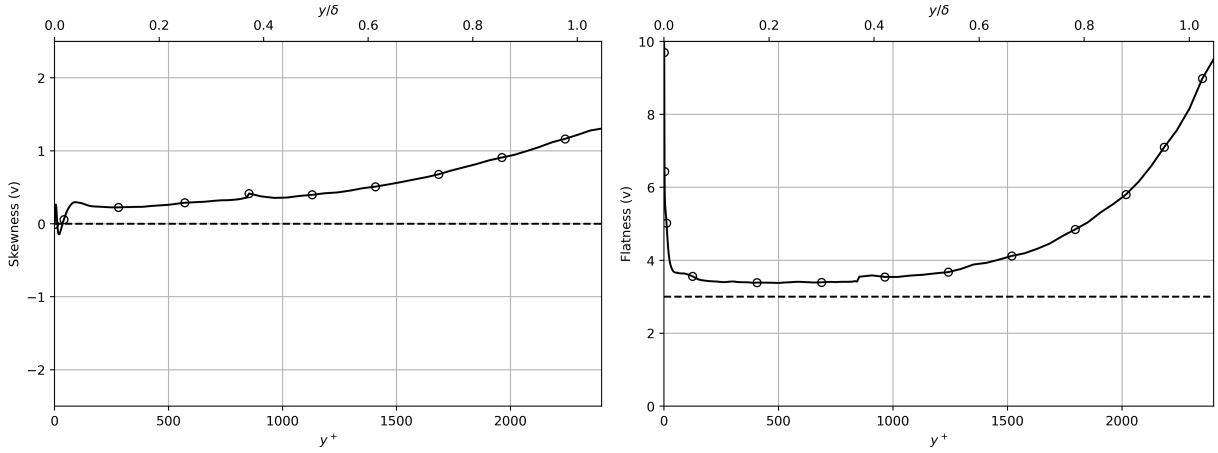

Fig. 12 Skewness and Flatness for the wall-normal velocity fluctuations.

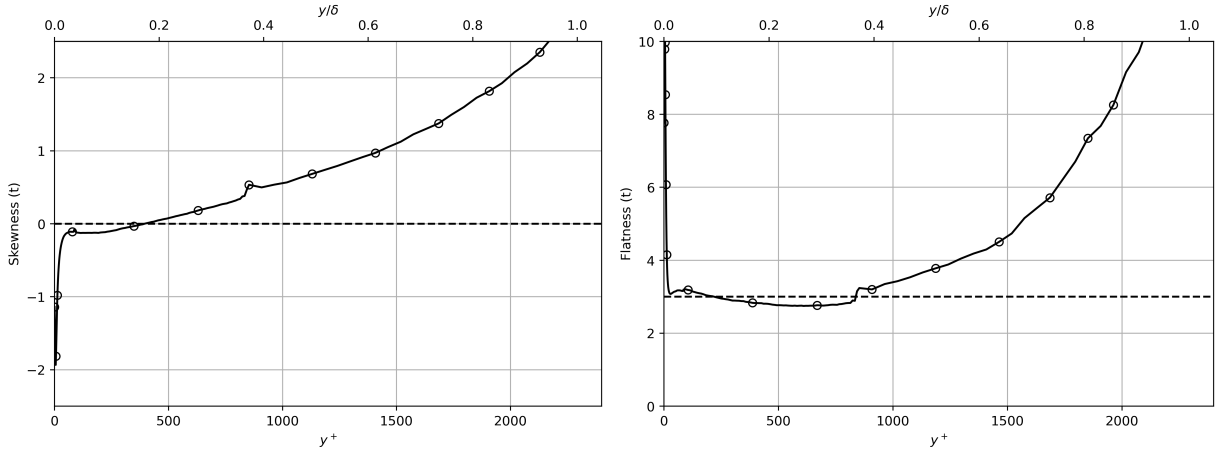

Fig. 13 Skewness and Flatness for the temperature fluctuations.

VI. Two-Point Cross-Correlations

In this section, we delve into the application of non-traditional two-point cross-correlations (TPCCs) for the identification and characterization of coherent structures in turbulent flows. Specifically, we focus on the two-point correlations of $u'v'$, $v'T'$, and $u'T'$, which offer unique insights into the relationships between velocity fluctuations, temperature fluctuations, and their interactions. These non-traditional correlations can provide valuable information regarding the momentum and heat transport processes, the dynamics of vortex stretching and compression, energy cascade mechanisms, and the spatial distribution of coherent structures, which are crucial in understanding the behavior of coherent structures and their impact on the flow dynamics. Additionally, we introduce the concept of two-point correlation of wall-pressure fluctuation with v' and p' throughout a volume. This technique enables the investigation of pressure-velocity interactions in the vicinity of the wall, which plays a significant role in the development and maintenance of coherent structures near the boundary. Furthermore, the wall-pressure fluctuation correlation can help to identify and understand the relationship between large-scale motions, pressure fluctuations, and the resulting wall-pressure distribution, which has a significant influence on the surface heat transfer and skin friction. By employing these advanced two-point correlation techniques, we can gain a deeper understanding of the underlying mechanisms driving the formation, evolution, and interaction of coherent structures in turbulent flows. These non-conventional

TPCCs provide a comprehensive perspective on the role of different flow variables in the dynamics of coherent structures, as well as the interplay between turbulent transport processes and the energy exchange among various scales of motion. In the following results, we will demonstrate the effectiveness of non-traditional TPCCs in capturing the complex behavior of coherent structures across various flow scenarios. Through the analysis of these non-conventional TPCCs, we aim to uncover key patterns, trends, and interactions among the velocity, temperature, and pressure fluctuations, shedding light on the underlying physics driving the formation and evolution of unconventional coherent structures in turbulent flows.

Experimentally gathering data inside the boundary layer for compressible, high-speed turbulent flows without perturbing the fluid flow is a challenging endeavour. However, wall measurements are relatively straightforward and can be used as a gateway to understanding the boundary layer behavior albeit indirectly. Figure 14 (a) depicts wall-pressure fluctuations at the reference point correlated to fluid pressure fluctuations in the domain. Moreover, the iso-surface of pressure correlations exhibits a concave curvature upstream of the reference point. The mushroom-like features bulge along the wall-normal direction with a convex curvature character downstream. Furthermore, figure 14 (b) depicts wall-pressure fluctuations at the reference point correlated to wall-normal velocity fluctuations. This cross-correlation exhibits very interesting features: the incident structure (blue) is negatively correlated above $y^+ = 4$. This structure is "reflected" (the angle of the two structures with respect to the plane is identical and equal to 51 deg (measured from the structure centerline). This angle is much more aggressive than the Mach angle for an isentropic expansion (20.5 deg) at $M_\infty = 2.86$. One possibility is that the observed reflection angle is not solely due to the primary pressure waves generated by the supersonic flow. It could also be influenced by secondary interactions between the wall, the turbulent structures, and other wave phenomena present in the flow. Furthermore, local variations in the flow properties, such as changes in the Mach number or pressure gradients, can also influence the wave propagation angles. The presence of local flow features, such as vortices, could introduce complex wave interactions that lead to the observed aggressive reflection angle. The negative correlations on the left leg of the "V" could indicate that there is an opposing relationship between wall pressure fluctuations and wall-normal velocity fluctuations in that region. This behavior might be related to the presence of coherent structures that are aligned in the streamwise direction, such as streamwise vortices, which can induce alternating high and low-pressure regions along with corresponding wall-normal velocity fluctuations. On the other hand, the positive correlations on the right leg of the "V" suggest that there is a more direct relationship between the wall pressure fluctuations and wall-normal velocity fluctuations in that region. This behavior could be associated with other types of flow structures, such as spanwise vortices or large-scale motions, which might create regions of high and low pressure that are more directly linked to the wall-normal velocity fluctuations.

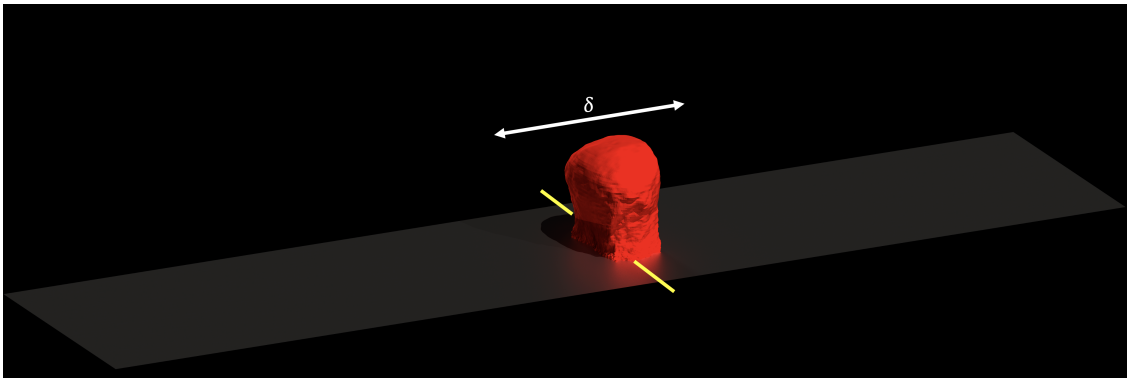

(a) $R_{p'_w p'}$

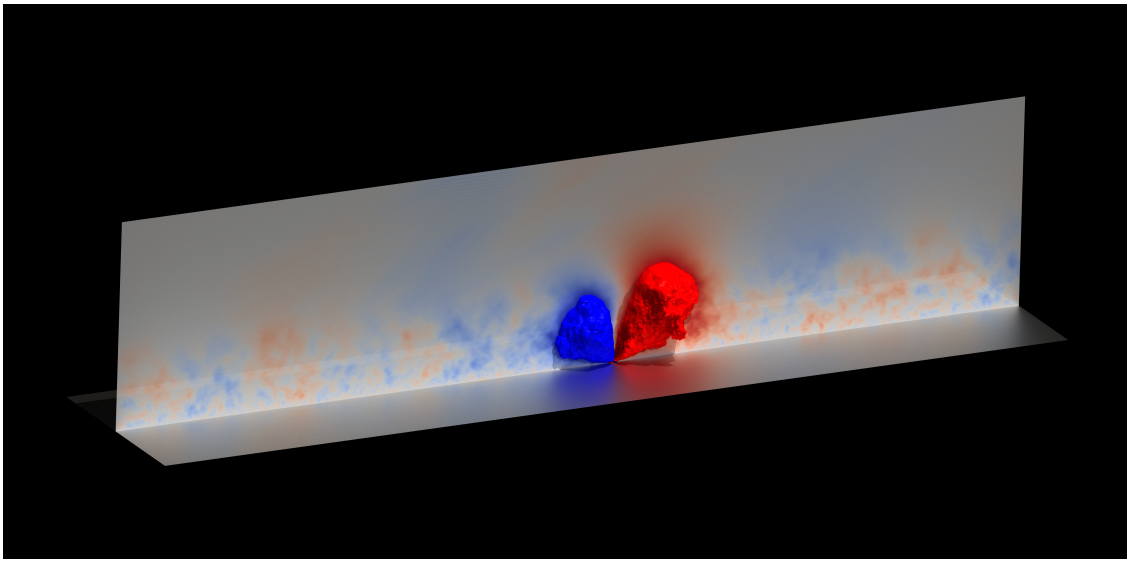

(b) $R_{p'_w v'}$. Note: streamwise intersection location coincides with reference station.

Fig. 14 (a) Two-point cross-correlation between wall pressure fluctuation at the reference point with pressure fluctuation in the domain. (b) Two-point cross-correlation between wall pressure fluctuation at the reference point with wall-normal velocity fluctuation in the domain. Note: the yellow line highlights the streamwise location for the TPCC and the white line provides a reference length in terms of the boundary layer thickness at the center of the domain or reference point.

Upon closer inspection in fig. 15, we can identify a two-layer phenomenon in the near-wall region ($y^+ \leq 4$) where the $p'_w v'$ correlation experiences a sign reversal. A two-layer situation in the two-point cross-correlation (TPCC) of wall pressure fluctuation and wall-normal fluctuation can arise due to the different dynamics governing the near-wall and outer regions of the turbulent boundary layer. The behavior of the correlations experiencing a reversal at $y^+ = 4$ may indicate a transition between these two regions, where different flow mechanisms dominate. In the near-wall region, the dynamics are largely influenced by the viscous effects, and the flow is predominantly governed by the wall shear stress. In the outer region, the influence of the wall diminishes, and the flow becomes more dominated by the inertial effects and large-scale turbulent structures. The reversal of the sign of the correlation in the near-wall region for the two-layer situation indicates that the relationship between wall pressure fluctuations and wall-normal velocity fluctuations undergoes a change as the flow transitions from the near-wall region to the outer region. The viscous sub-layer likely dampens the incoming waves resulting in a high-correlation in the vicinity of the wall between the wall and the incoming wave. In the outer region, the negative correlations on the left leg of the "V" could indicate that there is an opposing relationship between wall pressure fluctuations and wall-normal velocity fluctuations in that region. This behavior might be related to the presence of coherent structures that are aligned in the streamwise direction, such as

streamwise vortices, which can induce alternating high and low-pressure regions along with corresponding wall-normal velocity fluctuations. On the other hand, the positive correlations on the right leg of the "V" suggest that there is a more direct relationship between the wall pressure fluctuations and wall-normal velocity fluctuations in that region. This behavior could be associated with other types of flow structures, such as spanwise vortices or large-scale motions, which might create regions of high and low pressure that are more directly linked to the wall-normal velocity fluctuations. In summary, this TPCC configuration of $R_{p'_w p'}$ resembles a "quadrupole" with the streamwise axis located in the viscous sublayer around $y^+ \approx 4$. This phenomenon is unreachable by any fluid dynamics experimental technique due to its spatial resolution limitations, we have also observed a similar trend in our DNS case at $M_\infty = 2.86$ and lower Reynolds numbers.

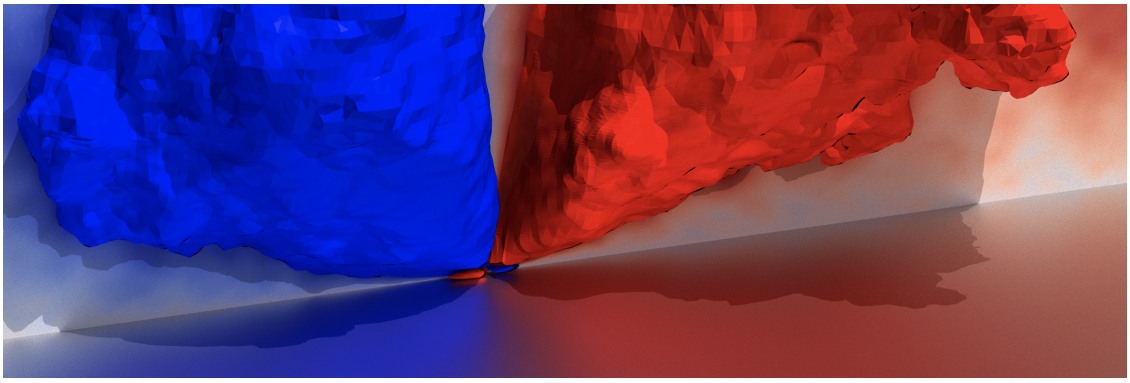

Fig. 15 Close-up of the inner-layer seen in the $R_{p'_w v'}$ correlation

The two-point cross-correlation $R_{u'v'}$, which represents the correlation between the streamwise velocity fluctuations (u') and the wall-normal velocity fluctuations (v'), provides unique insights into the momentum transfer by turbulent transport or mixing. In particular, it can help in identifying the key features such as ejections and sweeps, which are the principal turbulent events responsible for generating Reynolds shear stresses and turbulence production. Figure 16 shows extracted iso-surfaces of $R_{u'v'}$ for positive (red) and negative (blue) values at some strategic wall-normal locations inside the boundary layer: at $y^+ = 5$ (viscous sub-layer), 30 (peak location of $u'v'$) and 150 (log region). In all cases, TPCC threshold values for surface extraction range between 0.04 to 0.15 due to increased "noise" farther away from the wall and iLES. The TPCC results were normalized with the corresponding value at the reference point. First of all, the major turbulent $u'v'$ structure is negatively correlated (different from auto-correlations R_{uu} or R_{TT} as reported by [3]) due to the inherently anti-correlated behavior of u' and v' (Q2 events or ejections and Q4 events or sweeps mostly contribute to the Reynolds shear stress formation). Furthermore, as observed in 3D-TPC (i.e., R_{uu} and R_{TT}), the major structure is also flanked by two lateral sub-structures with opposite cross-correlation values (positive in this case). The principal negative-correlated structure clearly exhibits a wall-normal growth from the viscous sub-layer to the log region, also seen in the flanking structures. Furthermore, all $u'v'$ structures show that most of the influence zone in the near wall region is located downstream of the reference point, with their tails situated just upstream of the above mentioned point. The "picture" changes as one moves farther from the wall: the "zone of influence" and thus the structure "tails" move upstream. In addition, the Reynolds shear stress structures depict a more oblong silhouette in the buffer region and below with streamwise dimensions in the order of 1.5 to 2 δ's.

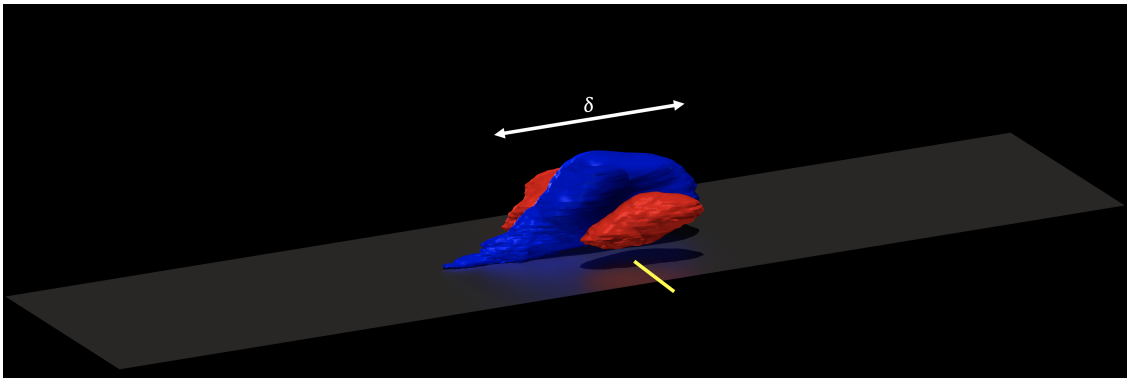

(a) $y^+ = 150$ (Log Region)

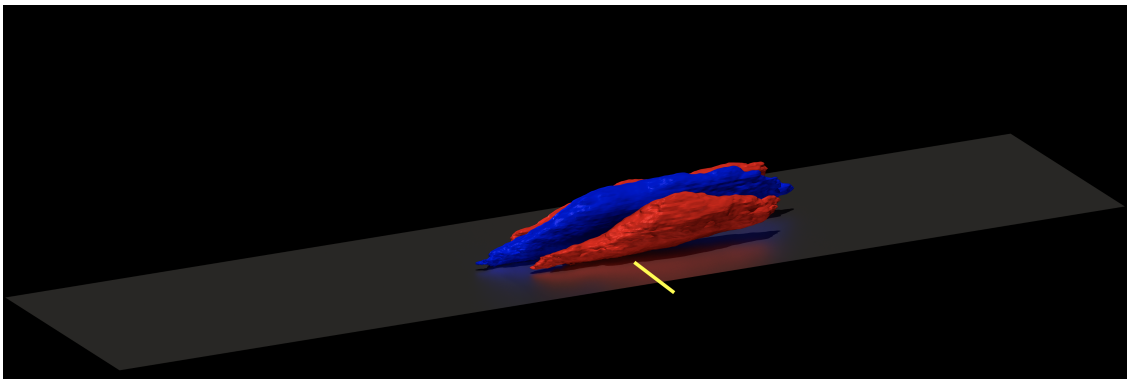

(b) $y^+ = 30$ (Peak $u'v'$ location at buffer region)

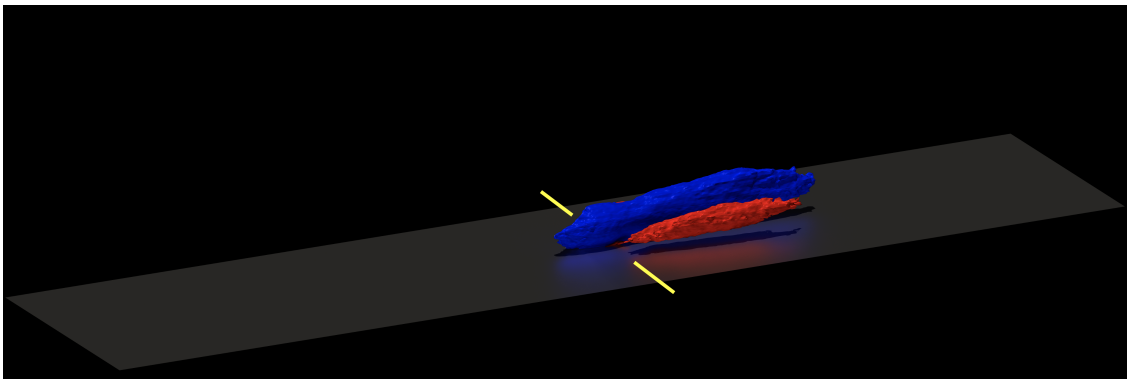

(c) $y^+ = 5$ (Viscous sub-layer)

Fig. 16 $R_{u'v'}$ two-point cross-correlations. Note: the yellow line highlights the streamwise location for the TPCC and the white line provides a reference length in terms of the boundary layer thickness at the center of the domain.

The $R_{v'T'}$ two-point cross-correlation, representing the correlation between the wall-normal velocity fluctuations (v') and temperature fluctuations (T'), offers a window into heat transfer mechanisms, mixing mechanics, thermal coherent structures and the coupling of momentum and heat transfer. Similar descriptive aspects discussed for $R_{u'v'}$ structures are applicable to $R_{v'T'}$ in terms of structure system configuration, zone of influence, and wall-normal growth. The most obvious distinction is related to the cross-correlation sign: the principal $R_{v'T'}$ structure is positive, and viceversa. This is explained by the fact that the static temperature decreases towards the boundary layer edge, i.e. $T_w > T_\infty$. Additionally, some degree of similarity can be traced between $R_{u'v'}$ and $R_{v'T'}$ TPCC volumes, which indicates that a Reynolds analogy can be defined for Reynolds shear stresses and wall-normal turbulent heat fluxes in supersonic

turbulent boundary layers.

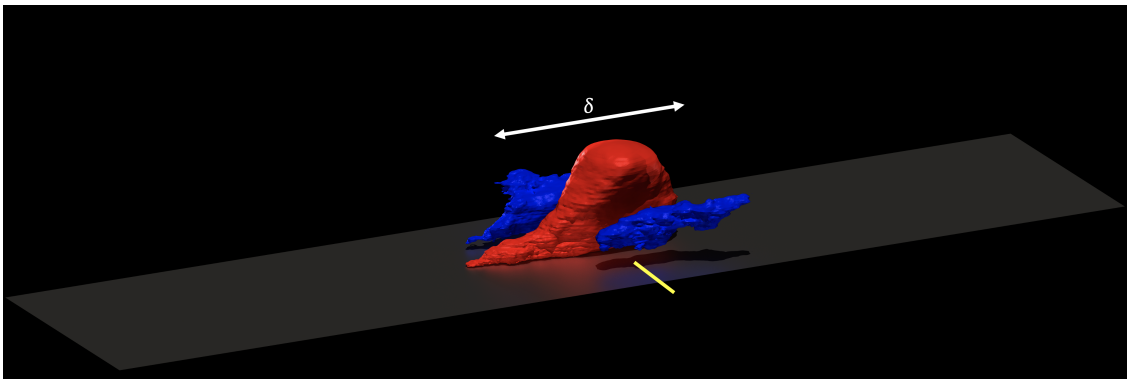

(a) $y^+ = 150$ (Log region)

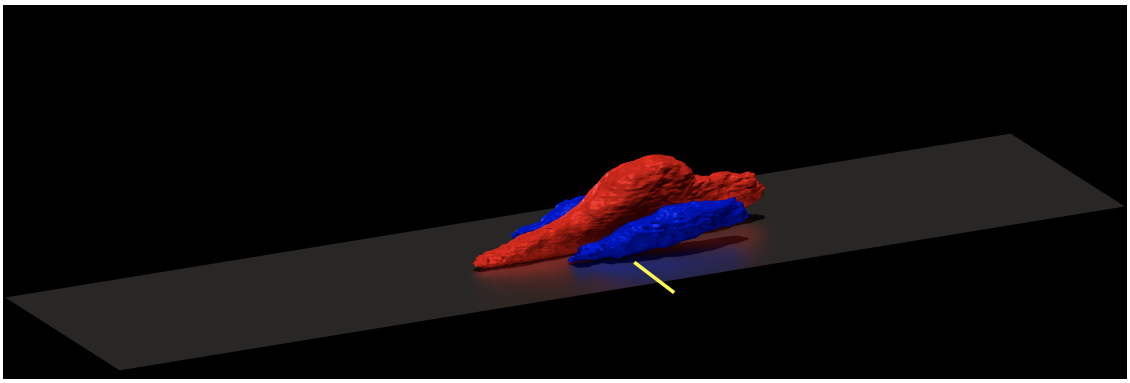

(b) $y^+ = 40$ (Peak $v'T'$ location at buffer region)

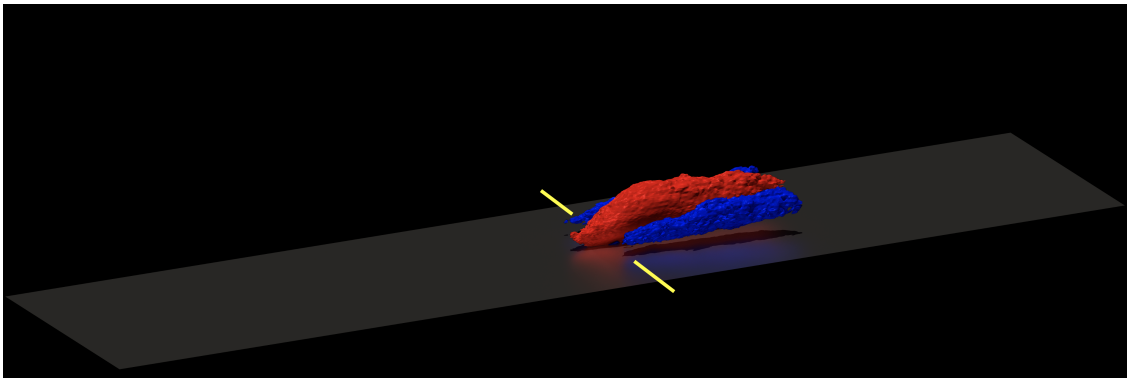

(c) $y^+ = 5$ (Viscous sub-layer)

Fig. 17 $R_{v'T'}$ two-point cross-correlations. Note: the yellow line highlights the streamwise location for the TPCC and the white line provides a reference length in terms of the boundary layer thickness at the center of the domain.

Analogous to $R_{v'T'}$, the $R_{u'T'}$ two-point cross-correlation, which represents the correlation between streamwise velocity fluctuations (u') and temperature fluctuations (T'), provides insights into the interactions between velocity and temperature structures in turbulent flows. Similarly, the focal point of the correlation is the coupling of heat and momentum transfer, which dictates the thermal energy transported or convected in the streamwise direction. Further, the $R_{u'T'}$ two-point correlation can be utilized to assess the validity of the Reynolds analogy, which posits a relationship between momentum and heat transfer in turbulent flows. This analogy assumes that the turbulent transport of momentum

and heat are proportional and similar, implying that the dimensionless skin friction coefficient and the dimensionless heat transfer coefficient are related. By examining the $R_{u'T'}$ correlation, we can gain insights into the relationship between streamwise velocity fluctuations and temperature fluctuations, which directly impact momentum and heat transfer processes. A strong correlation between u' and T' fluctuations would suggest that the Reynolds analogy holds true, as it indicates that momentum and heat are being transferred in a similar manner within the flow. Conversely, if the correlation is weak or exhibits a complex spatial distribution, this would imply that the Reynolds analogy might not be applicable in certain flow conditions or regions, as the transport mechanisms for momentum and heat could be significantly different. By carefully analyzing the $R_{u'T'}$ two-point correlation and comparing it with the predictions made by the Reynolds analogy, we can assess the extent to which the analogy is valid in describing the relationship between momentum and heat transfer in turbulent flows. This can provide valuable guidance for the development of turbulence models and the understanding of heat and momentum transport processes in complex flow scenarios. It is worth highlighting the very oblong silhouette of $R_{u'T'}$ in the buffer region and below, inside the boundary layer. Streamwise dimensions of $R_{u'T'}$ structures are in the order of 2.5 δ's or larger, confirming the high level of correlation between u' and T' (Reynolds analogy). Figure 19 shows the corresponding iso-surfaces of $R_{u'u'}$ in the log region. The similarity with $R_{u'T'}$ at the same wall-normal location is astonishing (excepting, of course, the correlation sign). In both cases, upstream tails reach the very near wall region (a turbulent eddy almost "attached" to the wall), although the reference point is located in the log region.

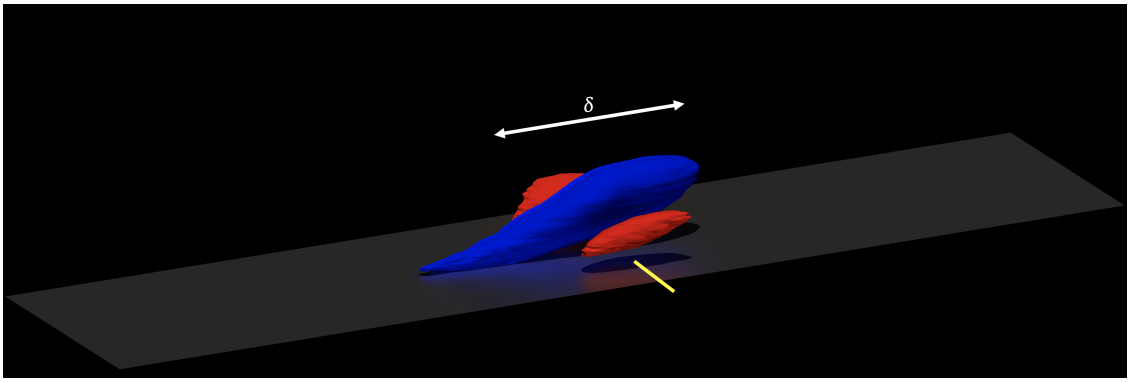

(a) y^+ = 150 (Log region)

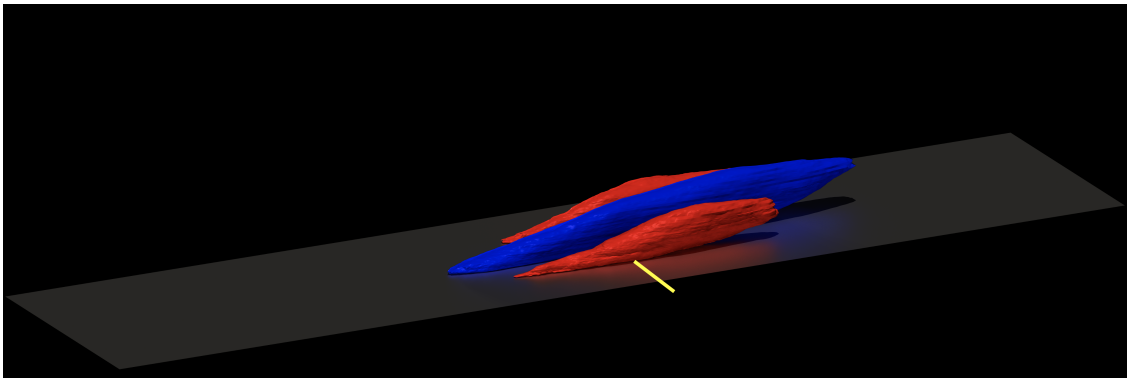

(b) y^+ = 15 (Peak $u'T'$ location at buffer region)

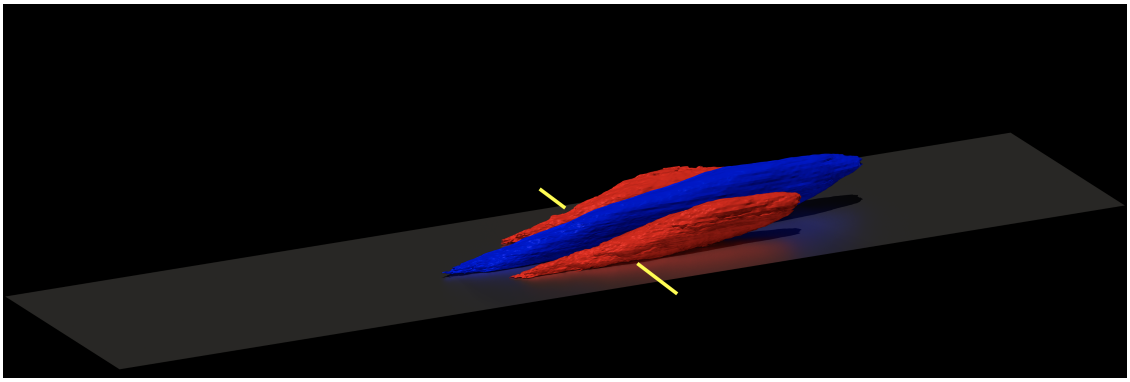

(c) y^+ = 5 (Viscous sub-layer)

Fig. 18 $R_{u'T'}$ **two-point cross-correlations. Note: the yellow line highlights the streamwise location for the TPCC and the white line provides a reference length in terms of the boundary layer thickness at the center of the domain.**

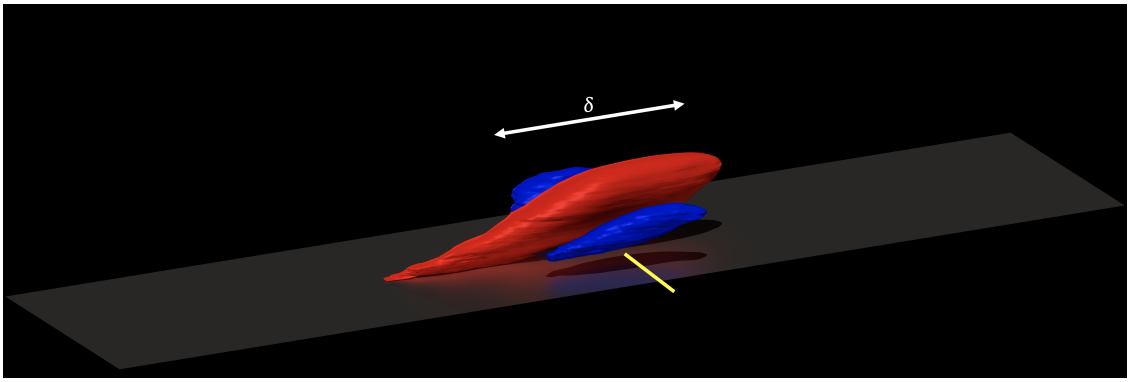

Fig. 19 $R_{u'u'}$ **two-point correlations at** $y^+ = 150$**. Note: the yellow line highlights the streamwise location for the TPC and the white line provides a reference length in terms of the boundary layer thickness at the center of the domain.**

VII. Conclusions

In this study, we have delved into the complex dynamics of supersonic turbulent boundary layers at a Mach number of 2.86, focusing on the statistical properties and two-point cross-correlations. Our analysis of higher-order statistics, namely skewness and flatness, has revealed significant deviations from Gaussian behavior, indicating the presence of intense, sporadic events and highlighting the intermittent nature of the turbulence. This intermittent behavior suggests a multifractal nature of the turbulence, implying a complex energy cascade process and scale-dependent statistical properties. The application of non-traditional two-point cross-correlations (TPCCs) has provided valuable insights into the relationships between velocity fluctuations, temperature fluctuations, and their interaction. These non-traditional correlations have shed light on the momentum and heat transport processes, the dynamics of vortex stretching and compression, energy cascade mechanisms, and the spatial distribution of coherent structures. Furthermore, the two-point correlation of wall-pressure fluctuation with v' and p' throughout a volume has enabled the investigation of pressure-velocity interactions in the vicinity of the wall, which plays a significant role in the development and maintenance of coherent structures near the boundary. Major findings are summarized as follows:

- Predicted skin friction coefficient, C_f, by SUPG-iLES is in excellent agreement with power-law curve fitting based on [60]'s experiments over supersonic adiabatic flat plates.
- The SUPG approach has demonstrated to be accurate not only in the near wall region for the mean streamwise velocity (i.e., wall-normal velocity gradient or C_f) but also in the entire turbulent boundary layer. Furthermore, the van Driest transformed velocity (U^+_{VD}) depicts a slightly longer power law behavior than its log-law counterpart (717 vs. 668 in wall units).
- The employed numerical dissipation scheme, i.e. SUPG, as SGS model has demonstrated an acceptable performance in high order statistics computation. The intermittency factor, which is inversely proportional to the flatness of streamwise velocity fluctuations, as predicted by iLES exhibited a very good agreement with DNS of [5] at Mach 3.
- Two-point cross-correlation of wall pressure fluctuations with domain pressure fluctuations has revealed the presence of a "quadrupole" in the viscous sub-layer, around $y^+ = 4$.
- Two-point cross-correlation of velocity and thermal fluctuations indicates more pronounced volume with high correlation values downstream of the reference point **in the viscous sub-layer**. Whereas, those volumes with high velocity-thermal correlations move upstream of the reference point (resembling very long and wall-attached tails) **in the buffer region and towards the boundary layer edge**. Furthermore, based on $R_{u'T'}$ structures, the high coherence observed between u' and T' implies that the Reynolds analogy still holds in supersonic turbulent boundary layers at $\delta^+ \approx 2{,}500$.

Despite the insights gained, our understanding of supersonic turbulent boundary layers remains incomplete. The complexity of these flows, characterized by a wide range of scales of motion and the presence of shock waves, presents significant challenges for both experimental and computational investigations. Future research should continue to leverage advanced diagnostic tools, such as those employed in this study, to further unravel the complex dynamics of these flows. In particular, the development of advanced turbulence models that can accurately capture the multifractal

nature and intermittent behavior of the turbulence will be crucial. Furthermore, the exploration of the relationship between large-scale motions, pressure fluctuations, and the resulting wall-pressure distribution holds significant potential for improving our understanding of surface heat transfer and skin friction in these flows. In conclusion, this study represents a step forward in our understanding of supersonic turbulent boundary layers. However, much work remains to be done. As we continue to unravel the complex dynamics of these flows, we move closer to the ultimate goal of predicting and controlling turbulence in supersonic flows, with significant implications for the design and operation of high-speed vehicles.

VIII. Acknowledgements

This material is based upon work supported by the National Science Foundation under grants #2314303, HRD-1906130, DGE-2240397. This material is based on research sponsored by the Air Force Research. Laboratory, under agreement number FA9550-23-1-0241. This work was supported in part by a grant from the DoD High-Performance Computing Modernization Program (HPCMP).

References

[1] Pope, S. B., *Turbulent Flows*, Cambridge University Press, 2000.

[2] Lagares, C. J., Rivera, W., and Araya, G., "Aquila: A Distributed and Portable Post-Processing Library for Large-Scale Computational Fluid Dynamics," *AIAA SciTech*, 2021.

[3] Lagares, C. J., and Araya, G., *Compressibility Effects on High-Reynolds Coherent Structures via Two-Point Correlations*, 2021. https://doi.org/10.2514/6.2021-2869, URL https://arc.aiaa.org/doi/abs/10.2514/6.2021-2869.

[4] Schlatter, P., and Orlu, R., "Assessment of direct numerical simulation data of turbulent boundary layers," *Journal of Fluid Mechanics*, Vol. 659, 2010, pp. 116–126.

[5] Bernardini, M., and Pirozzoli, S., "Wall pressure fluctuations beneath supersonic turbulent boundary layers," *Phys. Fluids*, Vol. 23, 2011, p. 085102.

[6] Grinstein, F., Margolin, L., and Rider, W., "Implicit large eddy simulation: computing turbulent fluid dynamics," *New York, NY: Cambridge University Press*, 2010.

[7] George, W., and Tutkun, M., "Mind the gap: a guideline for large eddy simulation," *Phil. Trans. R. Soc. A.*, Vol. 367, 2009, pp. 2839–2847.

[8] Sagaut, P., "Large Eddy Simulation for Incompressible Flows. An Introduction," *Measurement Science and Technology*, Vol. 12, No. 10, 2001, p. 1745.

[9] Lesieur, M., and Metais, O., "New Trends in Large-Eddy Simulations of Turbulence," *Annual Review of Fluid Dynamics*, Vol. 28, 1996, pp. 45–82.

[10] Porter, D. H., Pouquet, A., and Woodward, P. R., "Kolmogorov-like spectra in decaying three-dimensional supersonic flows," *Physics of Fluids*, Vol. 6, No. 6, 1994, pp. 2133–2142. https://doi.org/10.1063/1.868217.

[11] Grinstein, F. F., and DeVore, C. R., "Dynamics of coherent structures and transition to turbulence in free square jets," *Physics of Fluids*, Vol. 8, No. 5, 1996, pp. 1237–1251. https://doi.org/10.1063/1.868895.

[12] Fureby, C., and Grinstein, F., "Monotically Integrated Large Eddy Simulation of Free Shear Flows," *AIAA Journal*, Vol. 37, No. 5, 1999, pp. 544–556.

[13] Boris, J. P., "On large eddy simulation using subgrid turbulence models," *in Whither Turbulence. Turbulence at the Crossroads, ed. J. L. Lumley. New York: Springer-Verlag*, 1990, pp. 344–353.

[14] Boris, J., Grinstein, F., Oran, E., and Kolbe, R., "New insights into large eddy simulation," *Fluid Dynamics Research*, Vol. 10, No. 4, 1992, pp. 199–228. https://doi.org/https://doi.org/10.1016/0169-5983(92)90023-P.

[15] Oran, E., and Boris, J., "Computing Turbulent Shear Flows - A Convenient Conspiracy," *Computers in Physics*, Vol. 7, 1993, p. 523. https://doi.org/https://doi.org/10.1063/1.4823213.

[16] Urbin, G., and Knight, D., "Large-Eddy Simulation of a supersonic boundary layer using an unstructured grid," *AIAA Journal*, Vol. 39, No. 7, 2001, pp. 1288–1295.

[17] Stolz, S., and Adams, N., "Large-eddy simulation of high-Reynolds-number supersonic boundary layers using the approximate deconvolution model and a rescaling and recycling technique," *Physics of Fluids*, Vol. 15, No. 8, 2003, pp. 2398–2412.

[18] Lund, T., Wu, X., and Squires, K., "Generation of turbulent inflow data for spatially-developing boundary layer simulations," *Journal of Computational Physics*, Vol. 140, No. 2, 1998, pp. 233–258.

[19] Jansen, K. E., "A stabilized finite element method for computing turbulence," *Comp. Meth. Appl. Mech. Engng.*, Vol. 174, 1999, pp. 299–317.

[20] Jansen, K. E., Whiting, C. H., and Hulbert, G. M., "A generalized-α method for integrating the filtered Navier-Stokes equations with a stabilized finite element method," *Comp. Meth. Appl. Mech. Engng.*, Vol. 190, 1999, pp. 305–319.

[21] Rasquin, M., Smith, C., Chitale, K., Seol, S., Matthews, B., Martin, J., Sahni, O., Loy, R., Shephard, M., and Jansen, K., "Scalable fully implicit flow solver for realistic wings with flow control," *Computing in Science and Engineering*, Vol. 21, 2009, pp. 133–154.

[22] Tejada-Martinez, A., and Jansen, K., "A dynamic Smagorinsky model with dynamic determination of the filter width ratio," *Physics of Fluids*, Vol. 16, No. 7, 2004, pp. 2514–2528.

[23] Tejada-Martinez, A., and Jansen, K., "On the interaction between dynamic model dissipation and numerical dissipation due to streamline upwind/Petrov-Galerkin stabilization," *Computer Methods in Applied Mechanics and Engineering*, Vol. 194, 2005, pp. 1225 – 1248.

[24] Reed, W., and Hill, T., "Triangular mesh methods for the neutron transport equation," *Proc. Am. Nucl. Soc.*, Vol. 836, 1973, pp. 1–23.

[25] Stoter, S. K., Cockburn, B., Hughes, T. J., and Schillinger, D., "Discontinuous Galerkin methods through the lens of variational multiscale analysis," *Computer Methods in Applied Mechanics and Engineering*, Vol. 388, 2022, p. 114220. https://doi.org/https://doi.org/10.1016/j.cma.2021.114220, URL https://www.sciencedirect.com/science/article/pii/S004578252100551X.

[26] Cockburn, B., "Discontinuous Galerkin methods for computational fluid dynamics," *in: E. Stein, R. Borst, T. Hughes (Eds.), Encyclopedia of Computational Mechanics Second Edition. John Wiley & Sons, Ltd., Chichester, U.K.*, Vol. 5, 2018, pp. 141–203.

[27] Peraire, J., and Persson, P., "High-order discontinuous Galerkin methods for CFD," *in: Z.J. Wang (Ed.), Adaptive High-Order Methods in Computational Fluid Dynamics, Vol. 2, World Scientific*, Vol. 5, 2011, pp. 119–152.

[28] Huerta, A., Angeloski, A., Roca, X., and Peraire, J., "Efficiency of high-order elements for continuous and discontinuous Galerkin methods," *International Journal for Numerical Methods in Engineering*, Vol. 96, No. 9, 2013, pp. 529–560. https://doi.org/https://doi.org/10.1002/nme.4547, URL https://onlinelibrary.wiley.com/doi/abs/10.1002/nme.4547.

[29] Cockburn, B., Gopalakrishnan, J., and Lazarov, R., "Unified Hybridization of Discontinuous Galerkin, Mixed, and Continuous Galerkin Methods for Second Order Elliptic Problems," *SIAM Journal on Numerical Analysis*, Vol. 47, No. 2, 2009, pp. 1319–1365. https://doi.org/10.1137/070706616.

[30] Kirby, R., Sherwin, S., and Cockburn, B., "To CG or to HDG: A Comparative Study," *J. Sci Comput*, Vol. 51, 2012, pp. 183–212. https://doi.org/https://doi.org/10.1007/s10915-011-9501-7.

[31] Hughes, T. J. R., Oberai, A. A., and Mazzei, L., "Large eddy simulation of turbulent channel flows by the variational multiscale method," *Physics of Fluids*, Vol. 13, No. 6, 2001, pp. 1784–1799. https://doi.org/10.1063/1.1367868.

[32] Bazilevs, Y., Calo, V., Cottrell, J., Hughes, T., Reali, A., and Scovazzi, G., "Variational multiscale residual-based turbulence modeling for large eddy simulation of incompressible flows," *Computer Methods in Applied Mechanics and Engineering*, Vol. 197, No. 1, 2007, pp. 173–201. https://doi.org/https://doi.org/10.1016/j.cma.2007.07.016, URL https://www.sciencedirect.com/science/article/pii/S0045782507003027.

[33] Oberai, A., Liu, J., Sondak, D., and Hughes, T., "A residual based eddy viscosity model for the large eddy simulation of turbulent flows," *Computer Methods in Applied Mechanics and Engineering*, Vol. 282, 2014, pp. 54–70. https://doi.org/https://doi.org/10.1016/j.cma.2014.08.014, URL https://www.sciencedirect.com/science/article/pii/S0045782514002849.

[34] Martin, M. P., "Direct numerical simulation of hypersonic turbulent boundary layers. Part 1. Initialization and comparison with experiments," *Journal of Fluid Mechanics*, Vol. 570, 2007, pp. 347–364.

[35] Jansen, K., "Unstructured grid large eddy simulation of wall bounded flow," *Annual Research Briefs*, Center for Turbulence Research, NASA Ames / Stanford University, 1993, pp. 151–156.

[36] Whiting, C. H., Jansen, K. E., and Dey, S., "Hierarchical basis in stabilized finite element methods for compressible flows," *Comp. Meth. Appl. Mech. Engng.*, Vol. 192, No. 47-48, 2003, pp. 5167–5185.

[37] Whiting, C. H., "Stabilized finite element methods for fluid dynamics using a hierarchical basis," Ph.D. thesis, Rensselaer Polytechnic Institute, Sep. 1999.

[38] Hutchins, N., and Marusic, I., "Evidence of very long meandering features in the logarithmic region of turbulent boundary layers," *Journal of Fluid Mechanics*, Vol. 579, 2007, pp. 1–28.

[39] Hutchins, N., and Marusic, I., "Large-scale influences in near-wall turbulence," *Phil. Trans. R. Soc.*, Vol. 365, 2007, pp. 647–664.

[40] Araya, G., Castillo, L., Meneveau, C., and Jansen, K., " A dynamic multi-scale approach for turbulent inflow boundary conditions in spatially evolving flows," *Journal of Fluid Mechanics*, Vol. 670, 2011, pp. 518–605.

[41] Araya, G., Lagares, C., and Jansen, K., "Reynolds number dependency in supersonic spatially-developing turbulent boundary layers," *2020 AIAA SciTech Forum (AIAA 3247313) 6 - 10 January, Orlando, FL.*, 2020.

[42] Araya, G., Lagares, C., and Jansen, K., "Direct simulation of a Mach-5 turbulent spatially-developing boundary layer," *49^{th} AIAA Fluid Dynamics Conference, AIAA AVIATION Forum, (AIAA 3131876) 17 - 21 June, Dallas, TX*, 2019.

[43] Araya, G., Lagares, C., Santiago, J., and Jansen, K., "Wall temperature effect on hypersonic turbulent boundary layers via DNS," *AIAA Scitech 2021 Forum (AIAA-2021-1745)*, 2021. https://doi.org/10.2514/6.2021-1745.

[44] Lagares, C. J., and Araya, G., "Power spectrum analysis in supersonic/hypersonic turbulent boundary layers," *AIAA SciTech*, 2022.

[45] Xu, S., and Martin, M. P., "Assessment of inflow boundary conditions for compressible turbulent boundary layers," *Physics of Fluids*, Vol. 16, No. 7, 2004, pp. 2623–2639.

[46] Kistler, A., and Chen, W., "A Fluctuating Pressure Field in a Supersonic Turbulent Boundary Layer," *Journal of Fluid Mechanics*, Vol. 16, 1963, pp. 41–64.

[47] Zhou, M., Sahni, O., Shephard, M., Devine, K., and Jansen, K., "Controlling unstructured mesh partitions for massively parallel simulations," *SIAM J. Sci. Comp.*, Vol. 32, No. 6, 2010, pp. 3201–3227.

[48] Sahni, O., Luo, X., Jansen, K., and Shephard, M., "Curved boundary layer meshing for adaptive viscous flow simulation," *Finite Elements in Analysis and Design*, Vol. 46, No. 47-48, 2020, pp. 132–139.

[49] Chitale, K., Sahni, O., Shephard, M., Tendulkar, S., and Jansen, K., "Anisotropic Adaptation for Transonic Flows with Turbulent Boundary Layers," *AIAA Journal*, Vol. 53, 2015.

[50] Trofima, A., Tejada-Martinez, A., Jansen, K., and Lahey Jr, R., "Direct numerical simulation of turbulent channel flows using a stabilized finite element method," *Computers and Fluids*, Vol. 38, 2009, pp. 924–938.

[51] Sahni, O., Wood, J., Jansen, K., and Amitay, M., "Three-dimensional Interactions between a Finite-Span Synthetic Jet and a Cross Flow," *Journal of Fluid Mechanics*, Vol. 671, 2011, pp. 254–287.

[52] Vaccaro, J., Vasile, J., Olles, J., Sahni, O., Jansen, K., and Amitay, M., "Active Control of Inlet Ducts," *Int. J. of Flow Control*, Vol. 21, 2009, pp. 133–154.

[53] Vaccaro, J., Elimelech, Y., Chen, Y., Sahni, O., Jansen, K., and Amitay, M., "Experimental and Numerical Investigation on the flow field within a Compact Inlet Duct," *International Journal of Heat and Fluid Flow*, Vol. 44, 2014, pp. 478–488.

[54] Vaccaro, J., Elimelech, Y., Chen, Y., Sahni, O., Jansen, K., and Amitay, M., "Experimental and Numerical Investigation on Steady Blowing Flow Control within a Compact Inlet Duct," *International Journal of Heat and Fluid Flow*, Vol. 54, 2015, pp. 143–152.

[55] Sahni, O., Zhou, M., Shephard, M. S., and Jansen, K. E., "Scalable implicit finite element solver for massively parallel processing with demonstration to 160K cores," *Proceedings of the Conference on High Performance Computing Networking, Storage and Analysis*, 2009, pp. 68:1–68:12. https://doi.org/http://doi.acm.org/10.1145/1654059.1654129, URL http://doi.acm.org/10.1145/1654059.1654129.

[56] Rasquin, M., Smith, C., Chitale, K., Seol, E. S., Matthews, B. A., Martin, J. L., Sahni, O., Loy, R. M., Shephard, M. S., and Jansen, K. E., "Scalable Implicit Flow Solver for Realistic Wing Simulations with Flow Control," *Computing in Science & Engineering*, Vol. 16, No. 6, 2014, pp. 13–21. https://doi.org/10.1109/MCSE.2014.75.

[57] Lagares, C., Rivera, W., and Araya, G., "Scalable Post-Processing of Large-Scale Numerical Simulations of Turbulent Fluid Flows," *Symmetry*, Vol. 14, No. 4, 2022. https://doi.org/10.3390/sym14040823, URL https://www.mdpi.com/2073-8994/14/4/823.

[58] Abadi, M., Agarwal, A., Barham, P., Brevdo, E., Chen, Z., Citro, C., Corrado, G. S., Davis, A., Dean, J., Devin, M., Ghemawat, S., Goodfellow, I., Harp, A., Irving, G., Isard, M., Jia, Y., Jozefowicz, R., Kaiser, L., Kudlur, M., Levenberg, J., Mané, D., Monga, R., Moore, S., Murray, D., Olah, C., Schuster, M., Shlens, J., Steiner, B., Sutskever, I., Talwar, K., Tucker, P., Vanhoucke, V., Vasudevan, V., Viégas, F., Vinyals, O., Warden, P., Wattenberg, M., Wicke, M., Yu, Y., and Zheng, X., "TensorFlow: Large-Scale Machine Learning on Heterogeneous Systems," , 2015. URL https://www.tensorflow.org/, software available from tensorflow.org.

[59] "MPI: A message passing interface," *Supercomputing '93:Proceedings of the 1993 ACM/IEEE Conference on Supercomputing*, 1993, pp. 878–883. https://doi.org/10.1109/SUPERC.1993.1263546.

[60] Stalmach, C., "Experimental Investigation of the Surface Impact Pressure Probe Method Of Measuring Local Skin Friction at Supersonic Speeds," *Bureau of Engineering Research, University of Texas*, 1958.

[61] PIPONNIAU, S., DUSSAUGE, J., DEBIEVE, J. F., and DUPONT, P., "A simple model for low-frequency unsteadiness in shock-induced separation," *Journal of Fluid Mechanics*, Vol. 629, 2009, pp. 87–108.

[62] ELENA, M., and LACHARME, J., "Experimental study of a supersonic turbulent boundary layer using a laser doppler anemometer," *J. of Mec. Theor. Appl.*, Vol. 7, 1988, pp. 175–190.

[63] Bookey, P., Wyckham, C., Smits, A., and Martin, P., "New Experimental Data of STBLI at DNS/LES Accessible Reynolds Numbers," *43rd AIAA Aerospace Sciences Meeting and Exhibit, 10 - 13 January 2005, Reno, Nevada*, 2005, pp. AIAA 2005–309. https://doi.org/10.2514/6.2005-309.

[64] Donovan, J., Spina, E., and Smits, A., "The structure of a supersonic turbulent boundary layer subjected to concave surface curvature," *Journal of Fluid Mechanics*, Vol. 259, 1994, pp. 1–24.

[65] Frisch, U., *Turbulence: the legacy of A. N. Kolmogorov*, Cambridge university press, 1995.

[66] Antonia, R., and Chambers, A., "Intermittency in the region of the turbulent boundary layer," *Journal of Fluid Mechanics*, Vol. 55, No. 3, 1972, pp. 459–472.

[67] Kolmogorov, A., "A refinement of previous hypotheses concerning the local structure of turbulence in a viscous incompressible fluid at high Reynolds number," *J. Fluid Mech.*, Vol. 13, No. 1, 1962, pp. 82–85.

[68] Meneveau, C., and Sreenivasan, K., "The multifractal nature of turbulent energy dissipation," *J. Fluid Mech.*, Vol. 185, 1987, pp. 1–30.

[69] Schubauer, G. B., and Klebanoff, P. S., "Contributions on the Mechanics of Boundary-Layer Transition," *NACA-TR-1289*, 1955.

[70] White, F., *Viscous flow*, McGraw Hill, New York, 1974.